Article

Developmental Cell

Using an ER-specific optogenetic mechanostimulator to understand the mechanosensitivity of the endoplasmic reticulum

Graphical abstract

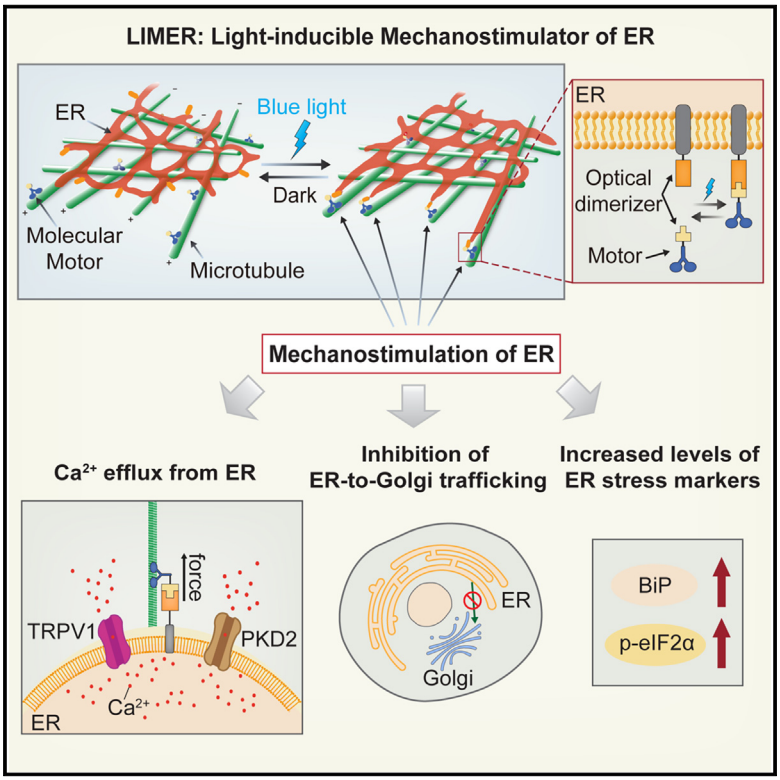

Highlights

- We developed an optogenetic ER-specific mechanostimulator, LIMER
- We revealed mechanosensitivity of ER and tight mechanoregulation of ER functions
- ER mechanostimulation elicits Ca^{2+} efflux from ER via TRPV1 and PKD2 channels
- It inhibits ER-to-Golgi trafficking and increases levels of ER stress markers

Authors

Yutong Song, Zhihao Zhao, Linyu Xu, ..., Yusong Guo, Xiaoqiang Yao, Liting Duan

Correspondence

ltduan@cuhk.edu.hk

In brief

Song et al. present an ER-specific optogenetic mechanostimulator named LIMER. Mechanostimulation of ER by using LIMER can induce Ca^{2+} release from ER, inhibit ER-to-Golgi trafficking, and increase levels of ER stress markers—providing direct proof for the mechanosensitivity of ER and the mechanoregulation of ER functions.

Song et al., 2024, Developmental Cell *59*, 1396–1409
June 3, 2024
https://doi.org/10.1016/j.devcel.2024.03.014

CellPress

CellPress
OPEN ACCESS

Developmental Cell

Article

Using an ER-specific optogenetic mechanostimulator to understand the mechanosensitivity of the endoplasmic reticulum

Yutong Song,[1,9] Zhihao Zhao,[1,9] Linyu Xu,[1,9] Peiyuan Huang,[1] Jiayang Gao,[2] Jingxuan Li,[3] Xuejie Wang,[4] Yiren Zhou,[4] Jinhui Wang,[4] Wenting Zhao,[5] Likun Wang,[6] Chaogu Zheng,[7] Bo Gao,[3] Liwen Jiang,[2] Kai Liu,[4,8] Yusong Guo,[4] Xiaoqiang Yao,[3] and Liting Duan[1,10,*]

[1]Department of Biomedical Engineering, The Chinese University of Hong Kong, Sha Tin, Hong Kong SAR 999077, China
[2]School of Life Sciences, Centre for Cell & Developmental Biology and State Key Laboratory of Agrobiotechnology, The Chinese University of Hong Kong, Sha Tin, Hong Kong SAR 999077, China
[3]School of Biomedical Sciences, The Chinese University of Hong Kong, Sha Tin, Hong Kong SAR 999077, China
[4]Division of Life Science, State Key Laboratory of Molecular Neuroscience, The Hong Kong University of Science and Technology, Kowloon, Hong Kong SAR 999077, China
[5]School of Chemical and Biomedical Engineering, Nanyang Technological University, Singapore 637457, Singapore
[6]National Laboratory of Biomacromolecules, CAS Center for Excellence in Biomacromolecules, Institute of Biophysics, Chinese Academy of Sciences, Beijing 100101, China
[7]School of Biological Sciences, Faculty of Science, The University of Hong Kong, Pok Fu Lam, Hong Kong SAR 999077, China
[8]Department of Chemical and Biological Engineering, The Hong Kong University of Science and Technology, Kowloon, Hong Kong SAR 999077, China
[9]These authors contributed equally
[10]Lead contact
*Correspondence: ltduan@cuhk.edu.hk
https://doi.org/10.1016/j.devcel.2024.03.014

SUMMARY

The ability of cells to perceive and respond to mechanical cues is essential for numerous biological activities. Emerging evidence indicates important contributions of organelles to cellular mechanosensitivity and mechanotransduction. However, whether and how the endoplasmic reticulum (ER) senses and reacts to mechanical forces remains elusive. To fill the knowledge gap, after developing a light-inducible ER-specific mechanostimulator (LIMER), we identify that mechanostimulation of ER elicits a transient, rapid efflux of Ca^{2+} from ER in monkey kidney COS-7 cells, which is dependent on the cation channels transient receptor potential cation channel, subfamily V, member 1 (TRPV1) and polycystin-2 (PKD2) in an additive manner. This ER Ca^{2+} release can be repeatedly stimulated and tuned by varying the intensity and duration of force application. Moreover, ER-specific mechanostimulation inhibits ER-to-Golgi trafficking. Sustained mechanostimuli increase the levels of binding-immunoglobulin protein (BiP) expression and phosphorylated eIF2α, two markers for ER stress. Our results provide direct evidence for ER mechanosensitivity and tight mechanoregulation of ER functions, placing ER as an important player on the intricate map of cellular mechanotransduction.

INTRODUCTION

The ability of cells to sense and respond to mechanical forces is critical for many cellular functions in various physiological and pathological conditions.[1,2] In the complex and compact intracellular environment, many cellular components contribute to the mechanics of cells and share the load of and react to mechanical stresses.[3,4] Decades of tremendous efforts have well established the roles of the cell membrane, cell cytoskeleton, and many signaling pathways in the complicated map of cellular mechanosensitivity and mechanotransduction. Recently, growing evidence also identifies the involvement of organelles. Forces received by cells can be propagated through cytoskeletal components to different intracellular organelles. The nucleus, as a crucial cellular mechanosensor, can respond to mechanical forces by altering nuclear envelope structure and composition, chromatin organization, and gene expression.[5] The mechanoregulation of other intracellular organelles is only beginning to be uncovered. Recent studies show that mitochondria undergo fission upon mechanostimulation.[6,7] Golgi has been found to respond to mechanical cues by modulating lipid metabolism.[8]

In contrast, little is known about the mechanosensitivity and mechanoresponding properties of the endoplasmic reticulum (ER). ER serves many critical roles in the cell, including calcium

(Ca^{2+}) storage, protein synthesis and transport, protein folding, and lipid and steroid synthesis.[9] ER is constantly exposed to differential intracellular forces, including forces generated by the movement of molecular motors attached to ER, the growth of microtubules coupled to ER, and the transport of ER-hitchhiked organelles.[10–12] On the other hand, extracellular mechanical cues can be transmitted to ER. For example, the deformation of ER structures can be observed when cells migrate over curved surfaces.[6] It has recently been found that mechanical stretching of the whole cell can result in the release of Ca^{2+} from the ER.[13] However, it is not clear whether this Ca^{2+} release is caused directly by mechanical perturbations of ER. Moreover, mechanosensitive ion channels such as transient receptor potential cation channel, subfamily V, member 1 (TRPV1), polycystin-2 (PKD2), and PANX-1 have been discovered to localize on ER membranes.[14–16] Despite accumulating yet indirect clues, direct evidence proving ER mechanosensitivity is not available.

One main challenge in elucidating ER mechanobiology is to apply forces directly and exclusively to ER, a large, temporally dynamic, and spatially heterogeneous network that is physically connected to many intracellular structures. Such ER-specific mechanostimulators are currently lacking. The commonly used force application methods include atomic force microscopy (AFM) and optical tweezers, which apply forces to cells via cantilevers or laser-maneuvered beads.[17,18] Recently, the random movement of pathogenic bacteria inside infected cells has been exploited to exert forces on any intracellular structures colliding with bacteria.[6] These methods all suffer from low-throughput and non-specific mechanostimulation of other intracellular components. To accurately dissect the role of ER in cellular mechanosensitivity and mechanotransduction, an ideal ER mechanostimulator would be ER-specific (not stimulating other structures), non-invasive, highly tunable, easy to obtain, high throughput, compatible with microscopy methods (allowing for simultaneous recording of ER responses), and would have spatiotemporal precision.

Here, to interrogate ER mechanosensitivity, we first developed an optogenetic ER-specific mechanostimulator, and next, we investigated the modulation of multiple ER functions by mechanical forces. Optogenetics has provided unprecedented solutions to modulate diverse intracellular activities remotely and precisely, including neuronal activities, intracellular signal transduction, gene expression, organelle transport, and phase separation, to name a few.[19–32] The ER-specific mechanostimulator we developed, referred to as a light-inducible mechanostimulator of ER (LIMER), utilizes blue light signals to drive the recruitment of molecular motors to ER, which applies the mechanical forces generated by motors directly and exclusively to ER without perturbing other intracellular structures. We demonstrated that LIMER enables force application toward ER with non-invasiveness, reversibility, high throughput, subcellular precision, as well as controllability in time and strength. Next, using LIMER, we identified that exerting mechanical force toward ER can induce a transient and rapid efflux of Ca^{2+} from ER. This Ca^{2+} efflux is dependent on the mechanosensitive cation channels TRPV1 and PKD2 in a cumulative way. Moreover, the mechanosensitive ER Ca^{2+} release can be repeatedly triggered and tuned by the intensity and duration of blue light. In addition, we found that mechanostimulation of ER can inhibit the ER-to-Golgi transport of secretory cargoes, and sustained mechanical stimuli on ER can increase the levels of binding-immunoglobulin protein (BiP) expression and phosphorylated eIF2α (p-eIF2α), two markers for ER stress. Our results provide direct proof for the mechanosensitivity of ER and the mechanoregulation of ER functions, presenting ER as an important player on the intricate map of cell mechanosensitivity and mechanotransduction.

RESULTS

The design and characterization of LIMER for mechanostimulation of ER

To construct the LIMER system, the optical dimerizer cryptochrome 2 (CRY2) and CIBN, which dimerize within milliseconds in the presence of blue light and dissociate after removal of blue light,[33–36] are utilized (Figure 1A). The photolyase homology region (PHR) of CRY2 is fused to the transmembrane domain of Sec61β that localizes on the ER membrane. CIBN, the N-terminal region of cryptochrome-interacting basic-helix-loop-helix 1 (CIB1), is fused to truncated kinesin-1 heavy-chain isoform KIF5A with the cargo-binding domain removed. Kinesins are a type of molecular motors that generate forces of several piconewtons and can move toward the plus end of microtubules with a speed of several hundred nanometers per second.[37] Using the two-component LIMER system, we hypothesize that upon blue light stimulation, motors will be recruited to the ER membrane via CRY2/CIBN association, thus applying the dragging forces toward ER.

To verify light-inducible mechanostimulation, COS-7 cells were co-transfected with CRY2-tdTomato-Sec61β, KIF5A-CIBN, and Tau-GFP, with tdTomato labeling ER structures and GFP marking microtubules via the microtubule-associated protein Tau. Upon blue light stimulation, ER tubules got stretched along the tracks of underlying microtubules, with tubules highlighted by arrows extending 5–10 μm within 12 s, confirming that kinesin-generated pulling forces are sufficient to deform ER (Figure 1B). Upon quantification, the average elongation speed of ER tubules across 99 ER tubules in 5 cells was 0.734 μm/s, aligning with kinesin's movement speed[37] (Figure 1C). During the mechanostimulation-triggered extension, one extending ER tubule could switch to another microtubule or be split into two (Figure S1A), which may possibly result from kinesin motors jumping between crossing microtubules.[38] Next, we showed that LIMER-mediated mechanostimulation could cause a drastic deformation of the whole ER network. Before blue light exposure, ER structures remained in their natural dynamic state where ER tubules were curved, forming relaxed lattice networks. Upon light stimulation, ER network was rapidly stretched out toward cell boundaries, leading to the gradually increased total ER network area (Figures 1D and 1E; Video S1). Close examination of the zoomed-in area indicated by the rectangle shows that ER tubules quickly elongated along microtubules and formed junctions with adjacent tubules (Figure 1F; Video S2). Consequently, the ER network extended into the cell periphery that was previously void of any ER structures. Quantification of the Mander's co-localization coefficient of ER and microtubule structures shows a continuous increase in overlap, confirming that microtubules serve as the scaffold for mechanostimulation-mediated ER remodeling (Figure 1G).

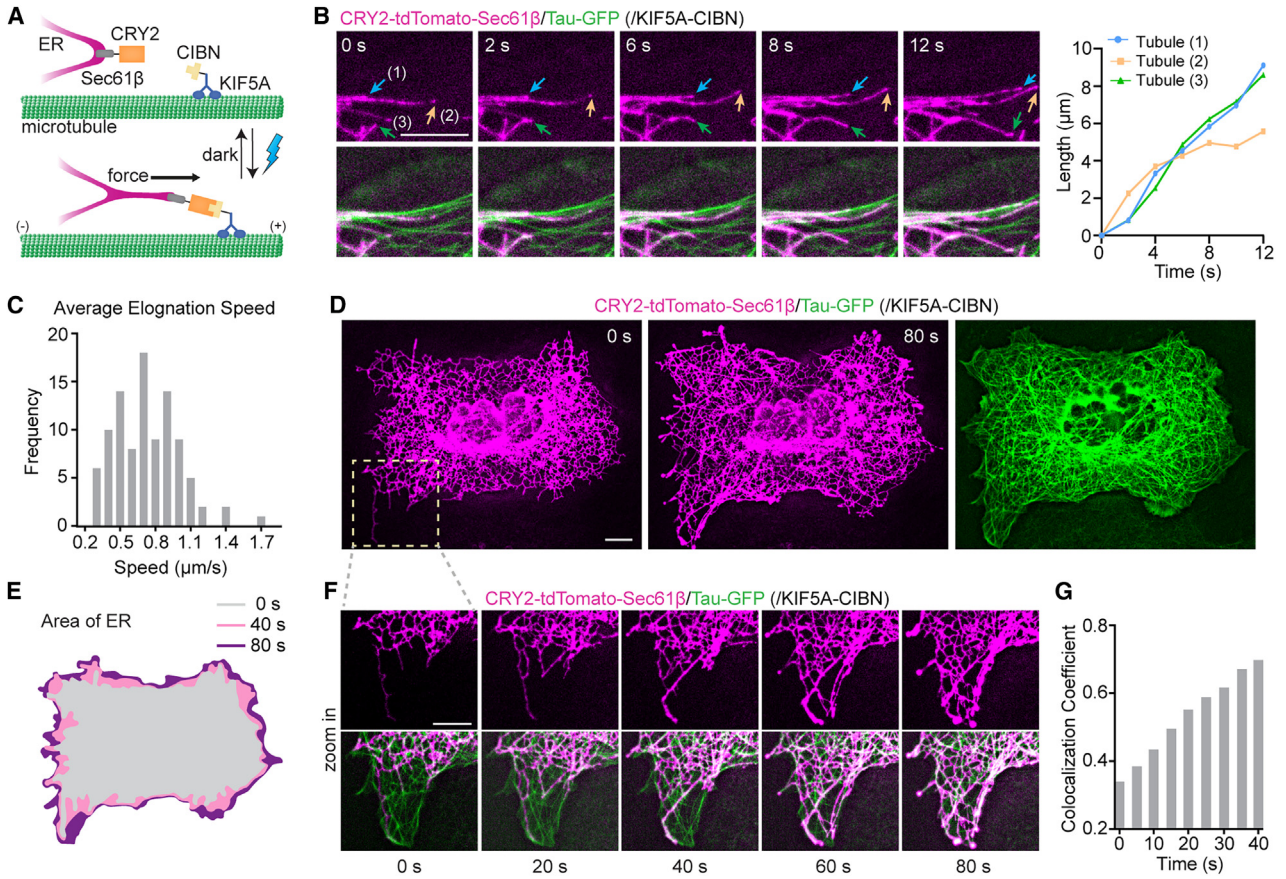

Figure 1. The design and characterization of LIMER for mechanostimulation of ER

(A) Schematic illustration of light-inducible mechanostimulation of ER (LIMER). Blue light induces CRY2 (fused with Sec61β) and CIBN (linked to KIF5A motors) interaction, directing forces of motors to ER membrane.

(B) Light-mediated force application induced ER tubule elongation. In COS-7 cells expressing CRY2-tdTomato-Sec61β, KIF5A-CIBN, and Tau-GFP, ER tubules were stretched by light-mediated force along the underlying microtubules (left), and their lengths were measured (right).

(C) Quantification of the speed of light-induced ER tubule elongation (n = 99 tubules, from 5 cells across 2 cultures).

(D) Light-mediated mechanostimulation induced stretching and deformation of ER network across the whole cell.

(E) Deformation caused the increase of ER area over time after light stimulation.

(F) In the marked area in (D), after blue light exposure, ER tubules were gradually stretching out toward the cell boundary along underlying microtubules while connecting with adjacent tubules, which resulted in the extension of the ER network.

(G) The level of co-localization increased over time as measured by Mander's co-localization coefficient of overlapping fluorescence signals between ER tubules and microtubules in (F).

200-ms pulses of 240 mW/cm^2 blue light at 2-s intervals were delivered to the whole cell. Scale bars, 10 μm. See also Figures S1 and S2 and Videos S1 and S2.

Moreover, light-inducible tubule extension and rearrangement occurred not only at the periphery but also in the middle of the ER network (Figures S1B and S1C). In control experiments where CRY2 was removed or replaced with the light-insensitive variant CRY2(D387A), blue light failed to induce any noticeable stretching or deformation of ER (Figure S1D). Moreover, by monitoring the ER dynamics in the same cell without or with blue light exposure, we found that ER tubules remained in their naturally relaxed and curved shape until the onset of blue light exposure, validating that the ER deformation was indeed driven by light-induced mechanostimulation (Figure S1D).

We further demonstrated that LIMER can serve as a modular platform. Another optical dimerizer (AsLOV2/ePDZ[39]), other motors (kinesin-1 heavy-chain isoforms: KIF5B [amino acid [aa] 1–807] and KIF5C [aa 1–560], or kinesin-3 motor KIF1A [aa 1–383]), or another ER-targeting sequence (the truncated cytochrome b5 protein [CB5], aa 100–134) can also be exploited to empower the light-mediated ER mechanostimulation (Figures S2A–S2E). The applicability of LIMER was further illustrated by its application in U2OS, PC3, and HeLa cells (Figures S2F–S2H), showing its potential as an adaptable and generalizable tool for photo-regulated ER mechanostimulation.

The reversible, temporal, and spatial control of mechanostimulation of ER

Using light signals as the trigger, LIMER can impart reversible, spatial, and temporal controllability over ER-targeted mechanostimulation. Light illumination can be precisely delivered to a target area at a particular time point for a desired duration. Light-mediated force application is reversible, with CRY2/CIBN

dissociating in the absence of blue light, allowing for repeated mechanostimulation. To examine the reversibility and temporal control, the cell expressing CRY2-tdTomato-Sec61β and KIF5A-GFP-CIBN was subject to a 100-ms blue light exposure at 0 min and another exposure at 32 min (Figure 2A; Video S3). The first exposure led to significant ER deformation. During the subsequent incubation without blue light, ER gradually recovered to a natural and relaxed morphology without obvious straightening and stretching tubules in around 15 min (Figure 2B). The results not only indicate the complete cessation of light-mediated mechanostimulation upon blue light withdrawal but also suggest the ability of ER structures to recover from force-induced rearrangement. Then, the second pulse of blue light re-elicited significant ER deformation, demonstrating the capability of LIMER to repeatedly exert forces onto ER at desired time points.

Furthermore, we have proved that light-gated mechanostimulation can be restricted to subcellular areas. As shown in Figure 2C and Video S4, blue light illumination was first confined to the region indicated by the blue box. As a result, stretching of ER tubules could be observed only within the illuminated area. Next, in the same cell, blue light delivery to another marked subcellular area resulted in ER deformation in that region, which has not been stimulated in the prior round of blue light illumination. Contrastingly, in the area highlighted by the yellow rectangle, which has not been exposed to any blue light stimulation throughout the experiment, the ER network remained unperturbed and relaxed, confirming the subcellular spatial precision of LIMER-mediated ER mechanostimulation. As a control, in COS-7 cells expressing CRY2(D387A)-integrated LIMER, neither repeated nor subcellular blue light stimulation caused any noticeable deformation of ER (Figure S1D).

Mechanostimulation of ER elicits Ca^{2+} release from ER via TRPV1 and PKD2

After establishing the LIMER system, we then set out to utilize it to explore the mechanosensitivity and mechanoregulation of ER by first probing how mechanostimulation of ER affects Ca^{2+} signaling. ER is known to be the main storage of Ca^{2+} in cells. Transfer of Ca^{2+} across the ER membrane is essential to regulating various cellular activities and maintaining intracellular Ca^{2+} homeostasis.[40,41] Although previous reports indicated that mechanical stress exerted on the whole cell induces ER Ca^{2+} signaling,[13] the direct proof linking ER mechanostimulation and ER Ca^{2+} signaling is missing. To fill the gap, we here used LIMER to administer forces directly to ER and simultaneously monitored the cytosolic Ca^{2+} concentration by GCaMP6, a genetically encoded intensiometric indicator that indicates cytosolic Ca^{2+} levels by green fluorescence.[42] In COS-7 cells expressing CRY2-tdTomato-Sec61β, KIF5A-CIBN, and GCaMP6, several seconds after blue light delivery, the cytosolic Ca^{2+} level rapidly and drastically increased and peaked around 20 s, which was followed by a subsequent decrease (Figure 3A; Video S5). This change in intracellular Ca^{2+} signaling indicated that ER is responsive to direct mechanical cues. In control experiments where cells expressed GCaMP6 only or non-functional LIMER systems with CRY2 removed or replaced with CRY2(D387A), no cytoplasmic Ca^{2+} increase was observed (Figures S3A–3C). In addition, integration of another photo-mediated hetero-dimerizing pair (LOVpep-ePDZ), other kinesin-1 isoforms (KIF5B and KIF5C), or kinesin-3 (KIF1A), or another ER-targeting sequence (CB5) in the LIMER system can also trigger cytoplasmic Ca^{2+} increases (Figures S3E–S3I). These results together validate that the Ca^{2+} increase indeed resulted from light-mediated ER mechanostimulation. In addition, the mechanical force-induced Ca^{2+} change can be observed in different types of cells, including U2OS, PC3, and HeLa cells (Figures S3J–S3L).

Next, we investigated the mechanisms of this force-triggered Ca^{2+} change. The pronounced light-induced Ca^{2+} increase was conserved after the removal of extracellular Ca^{2+} by using a Ca^{2+}-free medium, implying that this cytosolic Ca^{2+} increase originated from intracellular Ca^{2+} stores (Figure S4A). To check whether the cytosolic Ca^{2+} increase stemmed from Ca^{2+} efflux from ER, cells were treated with 3 μM thapsigargin (Tg) to deplete Ca^{2+} in ER lumen.[43] Tg treatment completely abolished the Ca^{2+} rise despite a significant light-mediated ER deformation (Figure 3B). Similarly, ATP treatment preceding blue light stimulation, which elicited ER Ca^{2+} release and thereby reduced the ER Ca^{2+} level, diminished the extent of the subsequent force-triggered Ca^{2+} change (Figure S4C). Moreover, the Ca^{2+} level in ER lumen, tracked by the intensiometric indicator G-CEPIA1er,[44] dropped upon light-gated increase of cytosolic Ca^{2+} (Figure S4B). Further confirming the reduced level of ER Ca^{2+} after light-mediated mechanostimulation, a prior blue light stimulation dampened the amplitude of cytosolic Ca^{2+} increase induced by subsequent ATP treatment (Figure S4D). Taken together, our results attest that force-induced cytosolic Ca^{2+} increase originated from ER Ca^{2+} release. Then we asked whether the applied force could cause ER membrane rupture and the ER Ca^{2+} release that arises from this rupture. Using transmission electron microscopy, we validated the continuity of the ER membrane after 15 min intermittent blue light stimulation (Figure S3M). In addition, no leakage of ER lumen-resident GFP was observed during light-mediated drastic ER deformation (Figure S3N). These results showed that light-mediated mechanostimulation over ER structures did not lead to ER membrane ruptures, and force-induced ER Ca^{2+} release was not a consequence of such ruptures.

We probed which Ca^{2+} channels were involved in the force-activated ER Ca^{2+} efflux, including TRPV1 and PKD2 (also called TRPP2) (Figures 3C–3E). These two Ca^{2+} channels were found to be localized on ER and are known to be mechanosensitive.[45,46] We used SB-366791, a selective TRPV1 antagonist, to block TRPV1.[47] Due to the lack of PKD2-specific inhibitors, the role of PKD2 was assessed by knocking down PKD2 expression with short hairpin RNA (shRNA). COS-7 cells were co-transfected with CRY2-tdTomato-Sec61β, KIF5A-CIBN, and GCaMP6. By measuring the kinetics of GCaMP6 signals, we found that temporal trends of cytosolic Ca^{2+} changes were similar among all the groups by reaching the peak around 20 s and then gradually dropping. However, cells treated with SB-366791 or PKD2 knockdown exhibited declined amplitudes of force-induced Ca^{2+} release, compared with non-treated or scrambled controls. By measuring ATP-induced Ca^{2+} changes in all groups to examine ER Ca^{2+} storages, we found that neither SB-366791 treatment nor PKD2 knockdown decreased the amount of Ca^{2+} stored in ER prior to mechanostimulation (Figures S4E–S4G). Therefore, our results show that TRPV1 and PKD2 participate in the force-induced ER Ca^{2+} release (Figure 3F). Additionally, it has been reported that

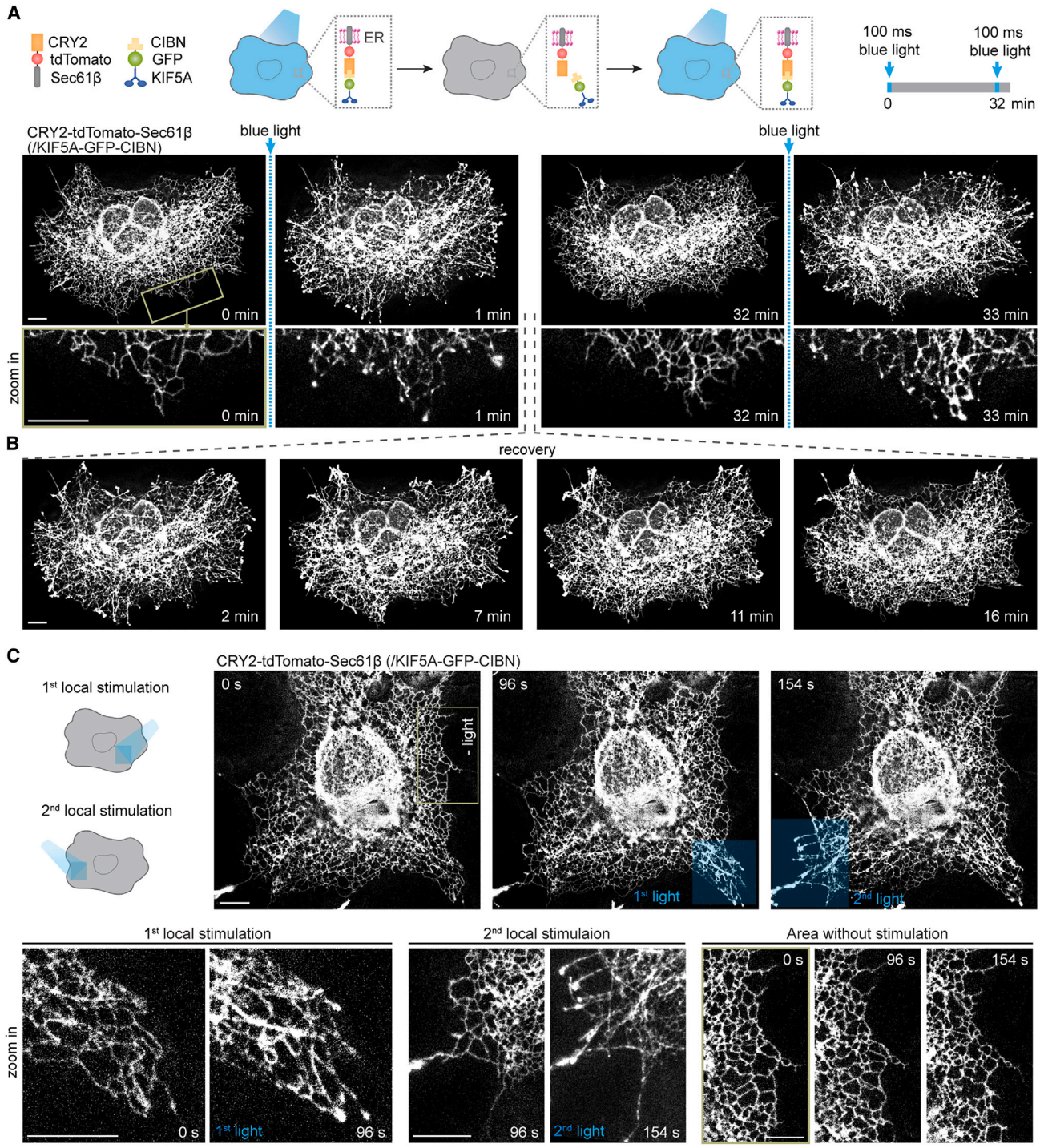

Figure 2. The temporal and spatial control of light-mediated ER mechanostimulation

COS-7 cells were transfected with CRY2-tdTomato-Sec61β and KIF5A-GFP-CIBN.

(A) Reversible and repeatable delivery of ER mechanostimulation. Due to reversible CRY2/CIBN association, light-induced ER mechanostimulation is reversible, ceasing without blue light and restarting upon re-exposure and leading to significant ER deformation with each light pulse at 0 and 32 min.

(B) During the stimulation interval devoid of any blue light exposure in (A), the mechanically stressed ER network gradually recovered to a relaxed shape.

(C) Subcellular spatial precision of ER mechanostimulation. The cell was subjected to two rounds of light stimulation restricted to different subcellular areas indicated by blue boxes (1st and 2nd). Each stimulation induced ER stretching and rearrangement in the targeted area, with the morphology of unilluminated ER remaining relaxed and unstretched.

One 100-ms pulse blue light (240 mW/cm^2) was delivered to (A) the whole cell or (C) subcellular regions marked by blue rectangles. Scale bars, 10 μm. See also Figure S1 and Videos S3 and S4.

CellPress
OPEN ACCESS

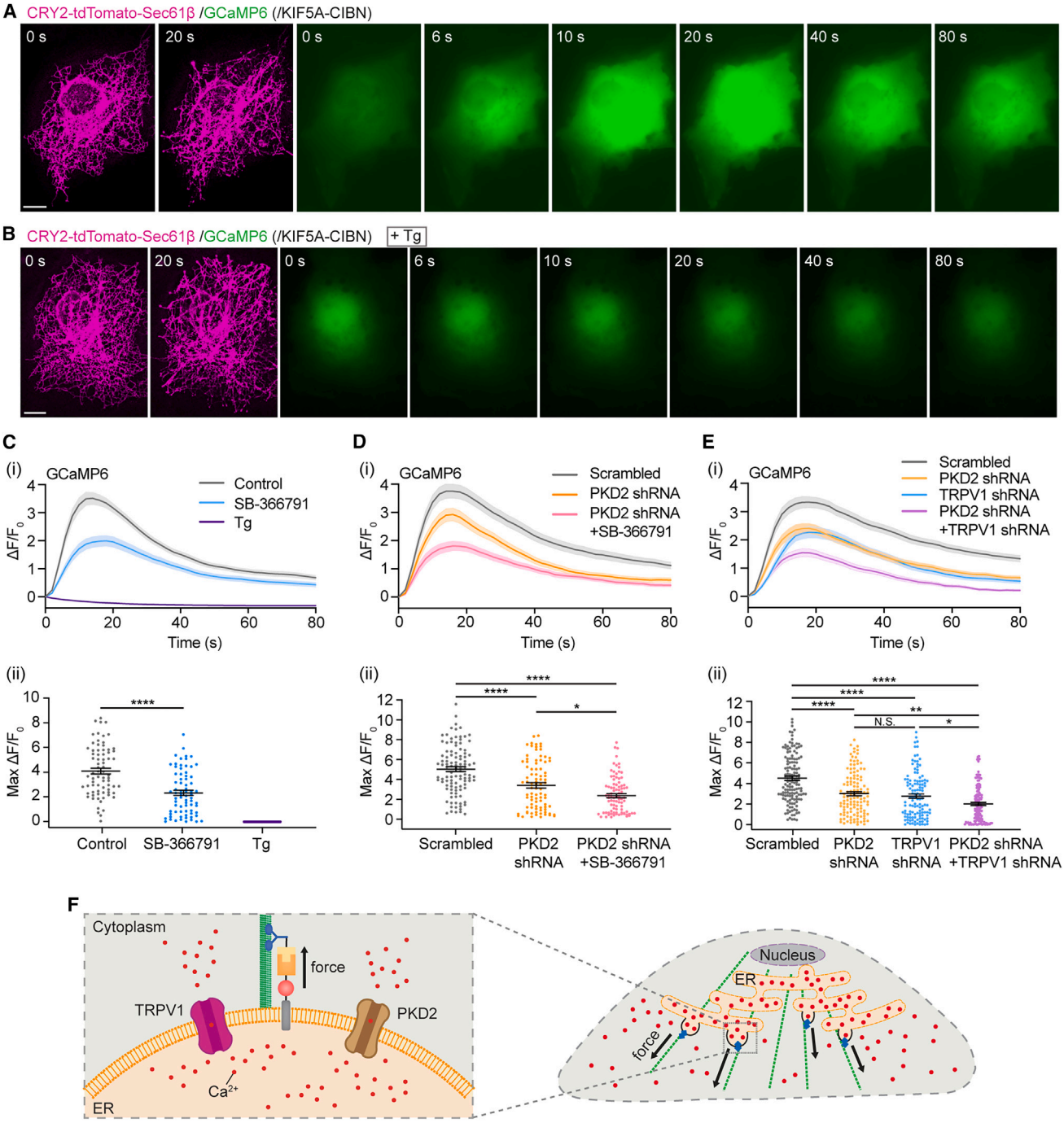

Figure 3. Mechanostimulation of ER elicits Ca^{2+} release from ER via TRPV1 and PKD2 channels

COS-7 cells were transfected with CRY2-tdTomato-Sec61β, KIF5A-CIBN, and GCaMP6.

(A) Upon ER mechanostimulation, the change of GCaMP6 intensity shows a rapid and transient increase in cytosolic Ca^{2+} level.

(B) With thapsigargin (Tg) treatment depleting ER Ca^{2+}, the cytosolic Ca^{2+} level did not increase after mechanostimulation as indicated by GCaMP6 intensity. 3 μM Tg was added to cells and incubated for 30 min in normal cell culture medium without EDTA before blue light stimulation.

(C) Upon ER mechanostimulation, Ca^{2+} kinetics illustrated by traces of relative change in GCaMP6 intensity ($\Delta F/F_0$) (i) and quantification of maximal Ca^{2+} change (illustrated by maximal $\Delta F/F_0$) (ii) for cells with no treatment (control), SB-366791 treatment, or Tg treatment.

(D) Upon ER mechanostimulation, Ca^{2+} kinetics illustrated by traces of GCaMP6 $\Delta F/F_0$ (i) and quantification of maximal Ca^{2+} change (illustrated by maximal $\Delta F/F_0$) (ii) for cells treated with scrambled shRNA, PKD2 shRNA for PKD2 knockdown, and a combination of PKD2 shRNA and SB-366791 for both PKD2 and TRPV1 inhibition.

(legend continued on next page)

PKD2 and IP3R interact with each other to modulate intracellular Ca^{2+} signaling.[48,49] Indeed, inhibition of IP3R by its inhibitor xestospongin C (XeC) or gene knockdown suppressed the force-induced ER Ca^{2+} release (Figure S6F), suggesting the involvement of IP3R. Moreover, combining XeC and PKD2 knockdown, which simultaneously inhibited IP3R and PKD2, did not further decrease the magnitude of Ca^{2+} efflux (Figure S6F), indicating that IP3R and PKD2 work via the same pathway to facilitate the force-induced ER Ca^{2+} release. In contrast, dual inhibition of TRPV1 and PKD2 with SB-366791 and PKD2 knockdown further reduced force-induced Ca^{2+} release than inhibiting either alone (Figure 3D). This result was corroborated by dual inhibition through TRPV1 knockdown and PKD2 knockdown (Figure 3E), showing that TRPV1 and PKD2 contribute to the force-induced ER Ca^{2+} release in a cumulative manner.

Mechanostimulation-induced ER Ca^{2+} release can be controlled in signaling amplitudes and repeatedly induced

We further checked whether and how the force-induced ER Ca^{2+} release could be triggered repeatedly and the signaling amplitude could be modulated by different strengths and durations of force application. To allow flexible adjustment of blue light illumination settings, we used jRGECO1a, a red fluorescence calcium indicator,[50] so that the spectra for recording Ca^{2+} changes and activating mechanostimulation were well separated. A single pulse of blue light was delivered to COS-7 cells expressing CRY2-GFP-Sec61β, KIF5A-CIBN, and jRGECO1a to activate ER mechanostimulation. First, we varied the duration of 48 mW/cm^2 blue light pulse from 100, 150, to 200 ms (Figures 4A and 4B). Then we fixed the exposure duration at 100 ms and altered the light intensity from 48 to 1,200 mW/cm^2 (Figures 4C and 4D). Light stimulation with a longer duration or a higher intensity induced cytosolic Ca^{2+} increases with higher amplitudes. Further extending the duration of one pulse blue light to 50 and 300 ms confirmed this trend (Figure S4H). The results demonstrated that the mechanosensitive ER Ca^{2+} signaling could be tightly tuned by different levels of mechanical perturbation.

Taking advantage of LIMER's temporal controllability, we probed whether and how the mechanostimulation-induced ER Ca^{2+} release can be repeatedly stimulated. The cell was exposed to the first pulse of blue light at 0 min and a second one at 16 min. Although both stimuli could trigger significant cytosolic Ca^{2+} rises, the amplitude of the second Ca^{2+} increase was lower than that of the first one (Figures 4E and 4F). Then we altered the intervals between the two stimuli from 2 to 60 min and quantified the kinetics of cytosolic Ca^{2+} changes as well as the ratios of the second amplitude over the first one (Figures 4G and 4H). Intervals of 6 min or longer could elicit a discernible second Ca^{2+} release, while shorter intervals could not. In addition, longer intervals produced a higher second cytosolic Ca^{2+} rise. The second Ca^{2+} elevation was lower than the first one when the intervals were 30 min or shorter (Figure S4I), possibly due to decreased ER Ca^{2+} storages or desensitization after the first stimulation. As a control, in COS-7 cells expressing CRY2(D387A)-integrated LIMER, either one pulse or two pulses of blue light did not evoke any noticeable cytosolic Ca^{2+} increase (Figure S3D). Our results demonstrated that force-induced ER Ca^{2+} release is repeatable and can be modulated in time and amplitude by differential force stimulation.

Mechanostimulation of ER inhibits the ER-to-Golgi transport

Next, we probed the influences of ER mechanostimulation on ER-to-Golgi trafficking. ER is the first station in the secretory pathway where newly synthesized proteins are incorporated into ER-derived carriers and transported to the Golgi before being sorted for delivery to their final destinations.[51] Prior research has linked ER membrane tension to ER-to-Golgi trafficking, suggesting a role for ER mechanics.[52] Here, we used the retention using selective hook (RUSH) assay to examine the efficiency of ER-to-Golgi transport in a synchronized manner.[53] Sonic hedgehog (Shh) is a key signaling molecule in embryonic patterning, cell differentiation, and organ development.[54] In the RUSH assay, the GFP-labeled N terminus of Shh (ShhN, aa 25–198) was fused with streptavidin-binding peptide (SBP) and stayed anchored in the ER by the streptavidin-KDEL hook.[55] Upon biotin addition, the ShhN reporter leaves ER and accumulates in the Golgi before being released from the cell (Figure 5A). We combined LIMER and RUSH to investigate how ER-targeted mechanostimulation affects ER-to-Golgi trafficking. Unexpectedly, overexpression of KIF5A fusion proteins caused significant Golgi fragmentation, which may interfere with RUSH assays, while the distributions and morphologies of other organelles, including the nucleus, peroxisomes, lysosomes, and mitochondria, were not affected (Figure S5C). In contrast, overexpression of KIF5B, KIF5C, and KIF1A did not fragment Golgi (Figure S5A). Therefore, we used KIF5C-integrated LIMER to deliver light-mediated mechanostimulation to ER. COS-7 cells were transfected with both RUSH and KIF5C-integrated LIMER systems. Before biotin addition, the ShhN reporter was localized in ER. Upon biotin addition, cells were kept in the dark or exposed to blue light illumination for 15 min before being fixed to examine ShhN distribution. In cells kept in the dark, most SBP-GFP-ShhN reached the Golgi 15 min after biotin addition (Figure 5C). However, in most cells stimulated by light, it was still trapped in ER, with only 27% of cells showing Golgi accumulation, compared with 78% in darkness (Figure 5B). The delayed ER-to-Golgi trafficking by ER mechanostimulation was also confirmed by live-cell imaging (Figure S5D). To rule out that blue light itself impeded the transport, we used the photo-insensitive CRY2 mutant CRY2(D387A) in LIMER, which did not affect ShhN delivery to the Golgi under light exposure (Figures 5D and S5D). Additionally, testing with the CB5-integrated or KIF1A-incorporated LIMER showed that light illumination

(E) Upon ER mechanostimulation, Ca^{2+} kinetics illustrated by traces of GCaMP6 $\Delta F/F_0$ (i) and quantification of maximal Ca^{2+} change (illustrated by maximal $\Delta F/F_0$) (ii) for cells treated with scrambled shRNA, PKD2 shRNA for PKD2 knockdown, TRPV1 shRNA for TRPV1 knockdown, and a combination of PKD2 shRNA and TRPV1 shRNA.

(F) Illustration scheme for mechanostimulation-induced Ca^{2+} release from ER via TRPV1 and PKD2 channels.

200-ms pulses of 240 mW/cm^2 blue light at 2-s intervals were delivered to the whole cell. Scale bars, 10 μm. Circles indicate measurements of individual cells. Traces and bars represent mean ± SEM. n > 70 from ≥3 independent experiments. The number of experiments, statistical tests, and exact p values are provided in Table S1 (N.S. $p > 0.05$, *$p < 0.05$, **$p < 0.01$, ****$p < 0.0001$). See also Figures S3, S4, and S6 and Video S5.

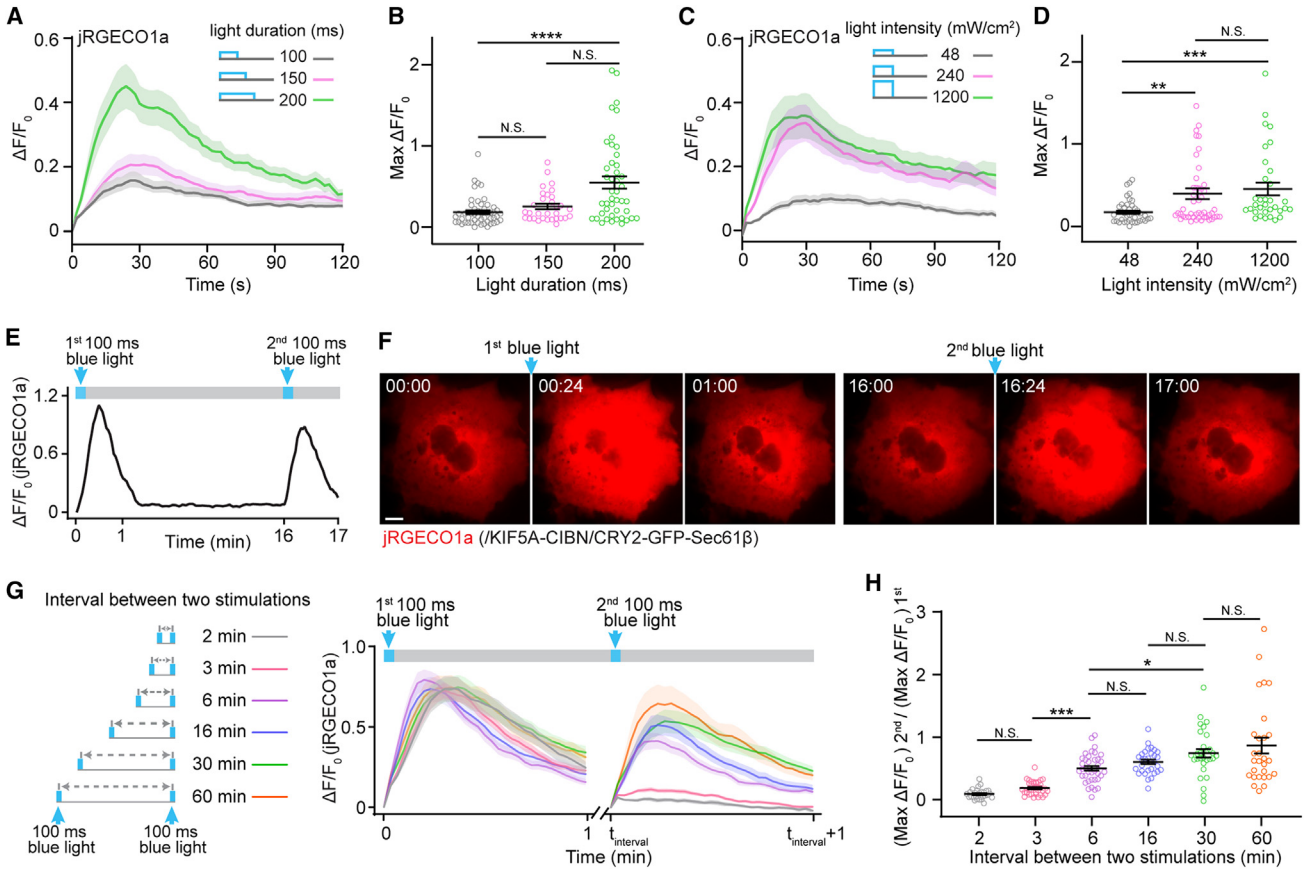

Figure 4. Mechanostimulation-induced ER Ca^{2+} release can be controlled in signaling amplitudes and repeatedly induced

COS-7 cells were transfected with CRY2-GFP-Sec61β, KIF5A-CIBN, and jRGECO1a

(A) Ca^{2+} kinetics illustrated by traces of jRGECO1a $\Delta F/F_0$ in cells exposed to one pulse of blue light at 48 mW/cm^2 for 100, 150, or 200 ms.

(B) Quantification of maximal Ca^{2+} change shows that a longer duration of light stimulation resulted in a higher amplitude of cytoplasmic Ca^{2+} increase.

(C) Ca^{2+} kinetics illustrated by traces of jRGECO1a $\Delta F/F_0$ in cells exposed to one pulse of 100 ms blue light at 48, 240, or 1,200 mW/cm^2.

(D) Quantification of maximal Ca^{2+} change shows that a higher intensity of light stimulation resulted in a higher amplitude of cytoplasmic Ca^{2+} rise.

(E) Ca^{2+} kinetics illustrated by traces of jRGECO1a $\Delta F/F_0$ in the cell shown in (F), exposed to two pulses of 100 ms blue light at t = 0 and t = 16 min, respectively.

(F) jRGECO1a intensity increased after each pulse of 100 ms blue light at 240 mW/cm^2.

(G) Ca^{2+} kinetics after two pulses of 100 ms blue light at 240 mW/cm^2, with intervals ranging from 2 to 60 min.

(H) Quantification of the ratio of maximal Ca^{2+} change induced by the second stimulation over that induced by the first stimulation.

Blue light stimulation was delivered to the whole cell. Scale bars, 10 μm. Circles indicate measurements of individual cells. Traces and bars represent means ± SEM, n > 28 from ≥2 independent experiments. The number of experiments, statistical tests, and exact p values are provided in Table S1 (N.S. p > 0.05, *p < 0.05, **p < 0.01, ***p < 0.001, ****p < 0.0001). See also Figures S3 and S4.

consistently decreased ER-to-Golgi transport (Figures S5E–S5H). Taken together, these results indicated that light-mediated mechanostimulation of ER inhibits the ER-to-Golgi transport.

Furthermore, we investigated whether the inhibitive effects of light-mediated mechanostimulation over the ER-to-Golgi transport involved force-induced Ca^{2+} signaling. To start with, we found that the release or depletion of ER Ca^{2+}, induced by the addition of ATP or Tg, respectively, did not affect ER-to-Golgi transport of ShhN (Figures 5E and S5B). Next, in cells expressing both LIMER and RUSH systems, treatment with Tg to deplete ER calcium did not prevent light-mediated mechanostimulation from hampering the ER-to-Golgi transport (Figure 5F). On the other hand, minimizing cytoplasmic Ca^{2+} increase by a membrane permeable Ca^{2+} chelator, BAPTA-AM, significantly hindered the ER-to-Golgi transport by itself (Figure 5E), in contrast to ATP or Tg treatment. However, BAPTA-AM treatment also failed to stop the force-induced inhibition of ER-to-Golgi transport (Figure 5F). Furthermore, light-mediated mechanostimulation still suppressed the transport after treatment with EGTA-AM, a slower Ca^{2+} chelator, or inhibition of PKD2 and TRPV1 individually or in combination (Figure S5I). Our results suggest that such force-mediated inhibition of ER-to-Golgi trafficking may not depend on the force-induced change of ER or cytosolic Ca^{2+}, raising intriguing questions on the underlying mechanisms, such as whether mechanostimulation can directly affect the functions of ER proteins involved in trafficking to inhibit transport. More future investigations are required to elucidate the underlying mechanisms.

Long-term mechanostimulation of ER increases expression of BiP and phosphorylation of eIF2α

We proceeded to explore the linkage between mechanical forces and ER stress. ER is known to act as the hub for protein

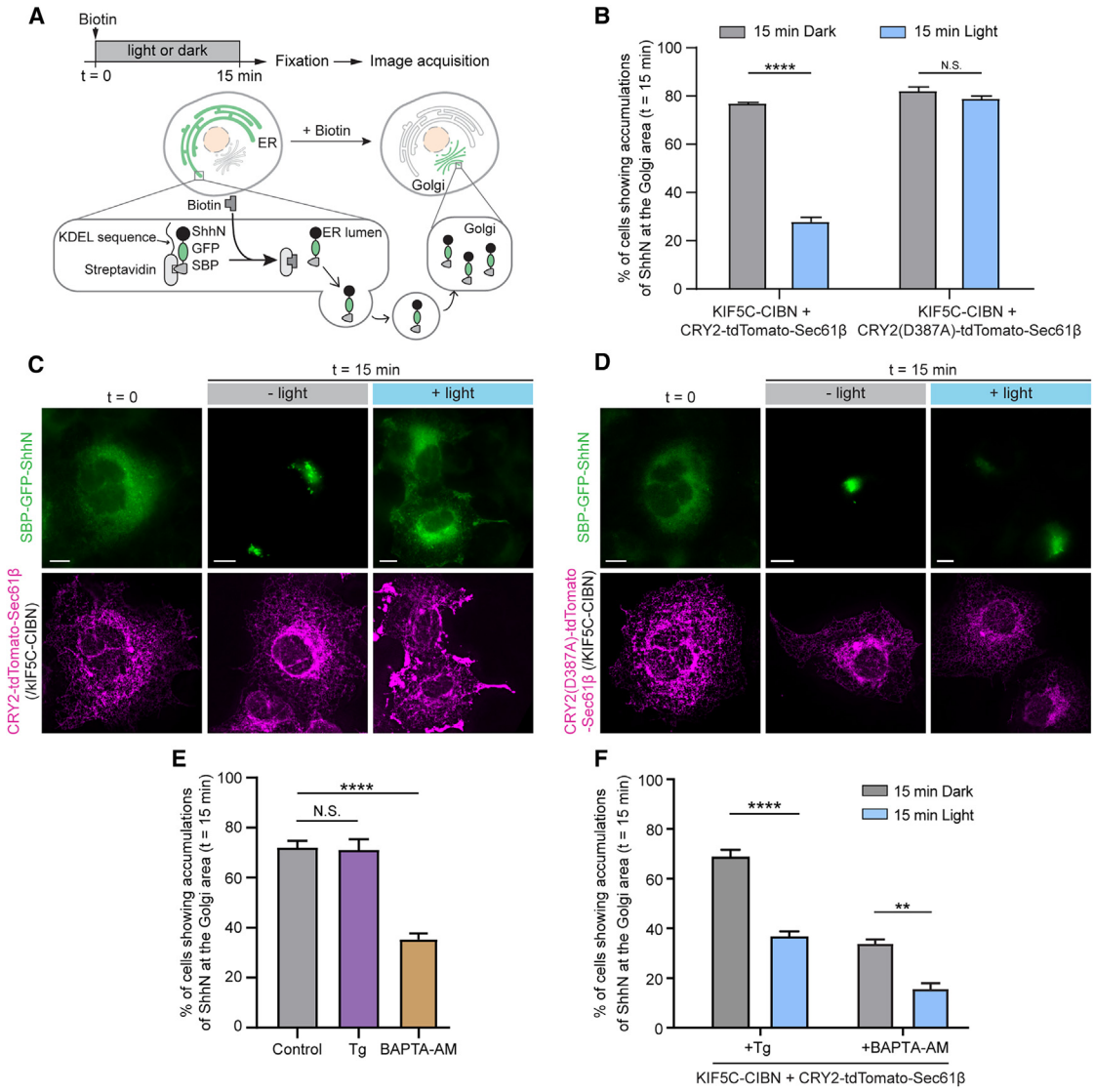

Figure 5. Mechanostimulation of ER inhibits ER-to-Golgi transport

(A) Illustrative scheme for RUSH assay. GFP-labeled ShhN reporters accumulate at Golgi after biotin addition, indicating successful ER-to-Golgi transport. Cells were fixed at t = 0 or 15 min after biotin addition with or without blue light exposure delivered to the whole culture (1 s on/4 s off intermittent blue light at 1 mW/cm^2 for 15 min).

(B) Analysis of SBP-GFP-ShhN trafficking using the RUSH system. COS-7 cells were transfected with both RUSH (Str-KDEL, SBP-GFP-ShhN) and LIMER (KIF5C-CIBN, CRY2-tdTomato-Sec61β, or the light-irresponsive CRY2(D387A)-tdTomato-Sec61β as a control).

(C) 15 min after biotin addition, cells unexposed to blue light exhibited reporter localization at Golgi, while cells that received light-mediated ER mechanostimulation did not.

(D) In the control group where light-mediated ER mechanostimulation was disabled by unfunctional CRY2(D387A), reporters translocated to Golgi with or without blue light stimulation.

(E) Analysis of SBP-GFP-ShhN trafficking using the RUSH system with or without thapsigargin (Tg) or BAPTA-AM treatment. COS-7 cells were transfected with RUSH (Str-KDEL, SBP-GFP-ShhN) and treated with 3 μM Tg or 50 μM BAPTA-AM for 30 min before biotin addition.

(F) Analysis of SBP-GFP-ShhN trafficking using the RUSH system with or without light-gated mechanostimulation after Tg or BAPTA-AM treatment. COS-7 cells were transfected with both RUSH (Str-KDEL, SBP-GFP-ShhN) and LIMER (KIF5C-CIBN, CRY2-tdTomato-Sec61β). After 3 μM Tg or 50 μM BAPTA-AM treatment for 30 min followed by biotin addition, cells were subject to 15 min of blue light illumination or kept in the dark.

Bars represent means ± SEM. n ≥ 4 for each group, each n represents a pool of ~150 transfected cells. The number of experiments, statistical tests, and exact p values are provided in Table S1 (N.S. $p > 0.05$, **$p < 0.01$, ****$p < 0.0001$). Scale bars, 10 μm. See also Figure S5.

folding. Excessive accumulation of misfolded polypeptides in ER gives rise to ER stress.[56] Previous reports found that mechanical stretching or mechanical stress loading exerted on the whole cell can elevate ER stress.[57,58] Here, we examined whether direct mechanostimulation of ER can affect ER stress by assessing the expression levels of BiP (also known as GRP-78), a major

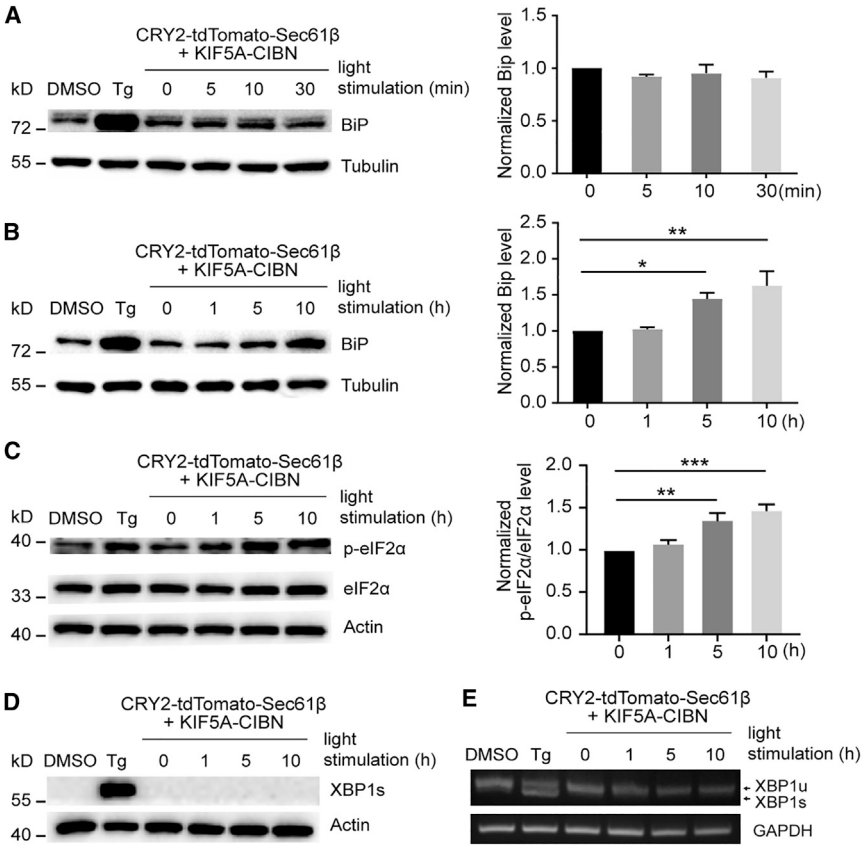

Figure 6. Long-term mechanostimulation of ER increases the expression of BiP and phosphorylation of eIF2α

COS-7 cells were transfected with CRY2-tdTomato-Sec61β and KIF5A-CIBN, and the whole cultures were exposed to intermittent blue light stimulation for 5–30 min (1 s on/4 s off intermittent blue light at 1 mW/cm^2) or 1–10 h (4 s on/4 min off intermittent blue light at 1 mW/cm^2). In COS-7 cells without any transfection, cells treated with Tg served as a positive control, and cells treated with DMSO as a negative control.

(A) Short-term light-mediated ER mechanostimulation for 5, 10, to 30 min did not induce noticeable changes in BiP levels. BiP levels were probed by western blotting assays and quantified as the ratio of BiP to tubulin (normalized by the t = 0 group).

(B) Long-term light-mediated ER mechanostimulation for 5 and 10 h led to significantly increased levels of BiP.

(C) Long-term light-mediated ER mechanostimulation for 5 and 10 h led to increased levels of p-eIF2α. p-eIF2α levels were probed by western blotting assays and quantified as the ratio of p-eiF2α to actin (normalized by the t = 0 group).

(D and E) Long-term light-mediated ER mechanostimulation for up to 10 h did not enhance the expression of spliced XBP-1 proteins as probed by western blotting assay (D) or the splicing of XBP1 mRNAs detected by RT-PCR (E). XBP1u, unspliced forms of XBP1 mRNAs; XBP1s, spliced forms of XBP1 mRNAs.

Bars represent means ± SEM, n ≥ 4 from 3 independent experiments. Groups were analyzed using one-way ANOVA with Dunnett's post hoc test (*p < 0.05, **p < 0.01, ***p < 0.001). See also Figure S6

ER chaperone that has been widely used as an ER stress marker in western blotting assays. First, we checked how mechanical stress in short durations affects BiP expression. COS-7 cells expressing LIMER were exposed to intermittent blue light stimulation for 0, 5, 10, or 30 min. The BiP expression levels were similar among the four different groups (Figure 6A). Next, we assessed the effects of long-term exertion of ER-targeted mechanostimulation by exposing the cells to intermittent blue light for 1, 5, or 10 h. As shown in Figure 6B, light illumination for 5 h resulted in elevated BiP expression, and the level got even higher for 10 h illumination. As a control, COS-7 cells expressing the CRY2(D387A)-integrated unfunctional LIMER did not exhibit any augmented BiP expression levels even after 10 h light stimulation (Figure S6A). The results confirmed that the increase of BiP expression indeed results from the ER-directed mechanostimulation over a prolonged duration.

Then, we asked whether force-induced Ca^{2+} change was implicated in the elevated BiP expression. Increasing evidence suggests that Ca^{2+} signaling plays a pivotal role in cell stress response.[59] It is well known that Tg induces ER stress by depleting ER calcium stores. The ER Ca^{2+} release induced by ATP also resulted in enhanced BiP expression level after 10 h (Figure S6B). After Tg treatment to deplete ER Ca^{2+}, long-term LIMER-mediated mechanostimulation did not increase the expression levels of BiP, compared with the corresponding dark control (Figure S6C). However, this result did not exclude the possibility that Tg treatment already evoked significantly high levels of BiP expression. Thus, any mild increase in BiP expression caused by LIMER-mediated mechanostimulation cannot be detected. On the other hand, BAPTA-AM treatment, by suppressing the cytosolic Ca^{2+} rise, inhibited the increase of BiP expression that could be induced by ER mechanostimulation (Figure S6D). This implies that an increase in cytosolic Ca^{2+} plays a significant role in ER mechanostimulation-triggered BiP expression.

Next, we investigated the upstream response of BiP expression caused by light-mediated ER mechanostimulation. Probed by western blot assay, the level of p-eIF2α slightly increased after 5 or 10 h of blue light stimulation (Figure 6C). Indeed, it has been previously found that the PERK-eIF2α pathway can upregulate the translation of a downstream transcription factor, which can activate the BiP promoter.[60] However, no noticeable XBP1 splicing was detected by western blot assay or reverse-transcription PCR (RT-PCR) after blue light stimulation for up to 10 h (Figures 6D and 6E). Nonetheless, the possibility exists that the ER stress, induced by light-mediated mechanostimulation, was sufficiently mild so that XBP1 splicing was not detected. On the other hand, there is a chance that the increased level of p-eIF2α may not stem from ER stress, as the phosphorylation of eIF2α can be triggered by various stresses via assorted pathways.[61] Collectively, our results suggest that long-term ER-directed mechanostimulation causes elevation of BiP expression and phosphorylation of eIF2α. Fully deciphering the mechanisms underlying cellular stress response to ER mechanostimulation of different durations merits further future investigations.

DISCUSSION

In this report, we presented an optogenetic ER-specific mechanostimulator (LIMER) that can exert mechanical forces specifically on intracellular ER, with non-invasiveness, reversibility, high throughput, subcellular precision, and controllability in time and strength. Next, with this new tool, we identified the mechanosensitivity of ER and the mechanoregulation of multiple ER functions. We found that mechanostimulation of ER can elicit a calcium efflux from ER, inhibit ER-to-Golgi trafficking, and induce ER stress, directly proving the ER mechanosensitivity and mechanoresponsiveness.

The long non-availability of tools to mechanically perturb intracellular ER prevents our exploration of ER mechanobiology. It is not surprising that such tools have been long lacking, considering that ER networks spread deep inside the cells and physically connect with diverse cellular components. It is impossible for all the current methods to precisely apply forces to ER without affecting other intracellular structures. LIMER, utilizing blue light to direct molecular motors' forces specifically to the ER, to our knowledge, is the first tool to precisely target ER in live cells without disturbing other structures. This method allows subcellular precision, is temporally controllable due to its reversibility, and is tunable in force intensity and duration. What's more, the delivery of light signals can be cheap, easy, and convenient. Both the light illumination and the production of genetically modified cells can be realized on large scales. Therefore, in comparison with other force application tools such as AFM or optical tweezers, which can only apply force to one cell at one time, LIMER can achieve high throughput by being able to stimulate many cells simultaneously. Moreover, LIMER can be combined with live-cell microscopy to examine how ER responds to mechanostimuli in real time. Therefore, we believe that LIMER can be a powerful tool to study ER mechanobiology and elucidate its role in the complex map of cell mechanotransduction.

We have demonstrated that different kinesins, membrane-targeting sequences, and other optogenetic hetero-dimerizing modules can be integrated into our strategy, which indicates that our design can serve as a general blueprint for realizing ER mechanostimulation. This versatility allows for our system to be tailored to specific research objectives. For example, red light-gated dimerizers, such as PHYB-PIF6, Bphp-PpsR2, and RedMap,[62–64] can be incorporated into LIMER for ER mechanostimulation with deeper tissue penetration or orthogonal control of other cellular processes. Different from using microtubule plus-end-directed kinesins, integrating minus-end-directed kinesin-14—via fusing ppKin14VIb[65] to CIBN—could retract some new ER tubules inward. However, the resulting ER deformation was less pronounced (Figures S2I and S2J), potentially due to the limited space available near the nucleus or to the anchoring of peripheral ER to other structures. Consequently, kinesin-14-based LIMER induced weaker ER mechanostimulation, potentially explaining its failure to trigger ER Ca^{2+} release or inhibit ER-to-Golgi trafficking (Figure S6E).

We found that mechanostimulation can induce a rapid ER Ca^{2+} release, which, for the first time, provides direct proof that intracellular ER is mechanosensitive and can respond to mechanical cues by Ca^{2+} signaling. We found that TRPV1 and PKD2 ion channels work additively, whereas PKD2 and IP3R operate on a common pathway for force-induced ER Ca^{2+} release, showcasing our method's capability to screen for mechanosensitive components in the ER. It is worth noting that even with combined inhibition of PKD2 and TRPV1, mechanostimulation still caused a slight ER Ca^{2+} release. This implies the possible involvement of other, yet unidentified, mechanosensitive players in ER, or it could also be due to incomplete inhibition of PKD2 and TRPV1. In addition, ER Ca^{2+} release or cytosolic Ca^{2+} increase itself did not deform the ER structures because the addition of ATP, capsaicin (the activator of TRPV1), or Tg did not induce noticeable ER deformation or stretching (Figure S1E). Despite those discoveries, several questions remain unanswered. What are the other mechanisms and mechanosensitive elements contributing to the mechanosensitivity of ER and the force-induced ER Ca^{2+} release? Why is the amplitude of Ca^{2+} rise in response to the second mechanostimulation lower than that induced by the first stimulation? Where are the destinations of Ca^{2+} ions that are being released from the mechanostimulated ER? More studies are needed to address these questions, which may be facilitated by LIMER. The mechanostimulation-triggered ER Ca^{2+} increase is independent of extracellular Ca^{2+}, opening new avenues to modulate various Ca^{2+} signaling-mediated biological processes in a manner independent of plasma membrane Ca^{2+} channels. On the other hand, ER structures are constantly exposed to different intracellular mechanical cues. Specifically, ER tubule elongation can be elicited by (1) forces provided by motors along microtubules, known as sliding, (2) attaching to polymerizing microtubules via specialized tip assembly complexes or (3) hitchhiking by associating with other organelles, such as lysosomes and early endosomes.[10–12] Our results also raise the possibility that the naturally occurring intracellular mechanostimulation of ER may contribute to the regulation of local Ca^{2+} inside the cells.

We further found that mechanical stimulation causes delays in ER-to-Golgi transport and leads to an increase in BiP expression and eIF2α phosphorylation. By examining the microtubule network after blue light stimulation, we found that the filament structures of microtubules were not disrupted (Figure S5J), indicating that the alterations in ER-to-Golgi transport and levels of ER stress markers were not caused by disruption of microtubule network. Although further investigations are required to uncover the exact mechanisms of how mechanical force affects ER stress or ER-to-Golgi transport, our results indicate the tight mechanoregulation of different aspects of ER functions. Whether other ER functions can be mechanomodulated remains unknown. Indeed, ER mechanobiology has been largely elusive and underexplored. How ER contributes to cell mechanosensitivity and mechanotransduction, either individually or jointly with other intracellular components, in various physiological and pathological settings, deserves further investigation to push the frontiers of cell mechanobiology.

In conclusion, we developed LIMER, a versatile method for ER-targeted mechanostimulation in live cells, offering unique advantages like remote control, non-invasiveness, reversibility, precision, and compatibility with any microscopes equipped with a blue light source. We envision that LIMER can greatly facilitate the study of ER mechanobiology and the exploration of the convoluted mechanotransduction network. Additionally, our results demonstrate that mechanostimuli can induce ER Ca^{2+} release through TRPV1 and PKD2 and can modulate ER functions, such as inhibiting ER-to-Golgi transport and affecting

stress responses, highlighting the ER's role in cellular mechanosensitivity and opening new avenues for further studies.

Limitations of the study

We identified that multiple aspects of ER functions can be regulated by mechanical forces. Future studies are needed to comprehensively understand the exact underlying mechanisms. Moreover, we noted that our study was done in cell lines. How ER perceives and responds to mechanical cues in primary cells and *in vivo* awaits more investigations.

Despite unique advantages, there are certain limitations in the LIMER strategy. First, it is challenging to control the exact location and direction of pulling forces exerted on ER. Whether and how a specific part of ER structures can receive mechanostimulation depends on the underlying, naturally formed microtubule structures that vary in the same cell and among different cells. An obvious tubule elongation and expansion of ER network induced by LIMER require two factors, an extended structure of microtubule network that serves as the scaffold guiding ER deformation and an original ER network not reaching boundaries of microtubule network. As a result, the extent of light-mediated ER tubule extensions varies from location to location and cell to cell. Additionally, quantifying and controlling the number of motor proteins engaged with the ER membrane, and thus the force exerted, remains difficult.

STAR★METHODS

Detailed methods are provided in the online version of this paper and include the following:

- KEY RESOURCES TABLE
- RESOURCE AVAILABILITY
  - Lead contact
  - Materials availability
  - Data and code availability
- EXPERIMENTAL MODEL AND SUBJECT PARTICIPANT DETAILS
  - Cell lines
- METHOD DETAILS
  - Plasmid Construction
  - Cell culture and transfection
  - Fluorescence live cell imaging
  - Treatments with drugs or with Ca^{2+}-free medium
  - Knockdown of PKD2, TRPV1, and IP3R3 in COS-7 cells
  - ATP-induced Ca^{2+} Release from ER
  - Retention Using Selective Hook (RUSH) Transport Assay and quantification
  - Immunoblotting
- QUANTIFICATION AND STATISTICAL ANALYSIS
  - Measurement of light-induced ER tubule elongation
  - Data Analysis for Ca^{2+} change
  - Statistical methods

SUPPLEMENTAL INFORMATION

Supplemental information can be found online at https://doi.org/10.1016/j.devcel.2024.03.014.

ACKNOWLEDGMENTS

We thank Prof. Yilin Wu for the discussion. This work was supported by National Natural Science Foundation of China (NSFC)-Young Scientists Fund (32201208 to L.D.), Young Collaborative Research Grant (YCRG) from the Research Grants Council (RGC) in Hong Kong (C4001-22Y to L.D.), National Natural Science Foundation of China/RGC Joint Research Scheme from RGC in Hong Kong (N_CUHK489/22 to L.D.), Guangdong Basic and Applied Basic Research Foundation (2023A1515011865 to L.D.), Collaborative Research Grant from RGC in Hong Kong (C6034-21G to K.L.), Guangzhou Key Projects of Brain Science and Brain-Like Intelligence Technology (20200730009 to K.L.), Innovation and Technology Commission (ITCPD/17-9 to K.L.), Research Impact Fund from RGC in Hong Kong (R4005-18F to X.Y.), Hong Kong Innovation and Technology Fund (ITS/212/21 to X.Y.), and a Direct Grant from the Chinese University of Hong Kong (4055172).

AUTHOR CONTRIBUTIONS

L.D., X.Y., Y.G., Y.S., Z.Z., and L.X. conceived the project and designed experiments. Y.S., Z.Z., L.X., P.H., J.G., X.W., J.L., Y.Z., and J.W. performed the experiments. All the authors discussed and analyzed the data. L.D., Y.S., Z.Z., and L.X. designed figures and wrote the manuscript, with input from all authors.

DECLARATION OF INTERESTS

The authors declare no competing interests.

Received: January 6, 2023
Revised: December 21, 2023
Accepted: March 8, 2024
Published: April 2, 2024

REFERENCES

1. Ingber, D.E. (2003). Mechanobiology and diseases of mechanotransduction. Ann. Med. *35*, 564–577. https://doi.org/10.1080/07853890310016333.
2. Jaalouk, D.E., and Lammerding, J. (2009). Mechanotransduction gone awry. Nat. Rev. Mol. Cell Biol. *10*, 63–73. https://doi.org/10.1038/nrm2597.
3. Wang, N., Butler, J.P., and Ingber, D.E. (1993). Mechanotransduction across the cell surface and through the cytoskeleton. Science *260*, 1124–1127. https://doi.org/10.1126/science.7684161.
4. Orr, A.W., Wayne Orr, A., Helmke, B.P., Blackman, B.R., and Schwartz, M.A. (2006). Mechanisms of Mechanotransduction. Dev. Cell *10*, 11–20. https://doi.org/10.1016/j.devcel.2005.12.006.
5. Maurer, M., and Lammerding, J. (2019). The Driving Force: Nuclear Mechanotransduction in Cellular Function, Fate, and Disease. Annu. Rev. Biomed. Eng. *21*, 443–468. https://doi.org/10.1146/annurev-bioeng-060418-052139.
6. Helle, S.C.J., Feng, Q., Aebersold, M.J., Hirt, L., Grüter, R.R., Vahid, A., Sirianni, A., Mostowy, S., Snedeker, J.G., Šarić, A., et al. (2017). Mechanical force induces mitochondrial fission. eLife *6*, e30292. https://doi.org/10.7554/eLife.30292.
7. Liu, X., Xu, L., Song, Y., Li, X., Wong, C.-Y., Chen, R., Feng, J., Gou, Y., Qu, Y., Chow, H.-M., et al. (2024). Force-induced tail-autotomy mitochondrial fission and biogenesis of matrix-excluded mitochondrial-derived vesicles for quality control. Proc. Natl. Acad. Sci. USA *119*, e2217019121. https://doi.org/10.1073/pnas.2217019121.
8. Romani, P., Brian, I., Santinon, G., Pocaterra, A., Audano, M., Pedretti, S., Mathieu, S., Forcato, M., Bicciato, S., Manneville, J.B., et al. (2019). Extracellular matrix mechanical cues regulate lipid metabolism through Lipin-1 and SREBP. Nat. Cell Biol. *21*, 338–347. https://doi.org/10.1038/s41556-018-0270-5.
9. Schwarz, D.S., and Blower, M.D. (2016). The endoplasmic reticulum: structure, function and response to cellular signaling. Cell. Mol. Life Sci. *73*, 79–94. https://doi.org/10.1007/s00018-015-2052-6.

10. Goyal, U., and Blackstone, C. (2013). Untangling the web: mechanisms underlying ER network formation. Biochim. Biophys. Acta *1833*, 2492–2498. https://doi.org/10.1016/j.bbamcr.2013.04.009.

11. Zajac, A.L., Goldman, Y.E., Holzbaur, E.L.F., and Ostap, E.M. (2013). Local Cytoskeletal and Organelle Interactions Impact Molecular-Motor-Driven Early Endosomal Trafficking. Curr. Biol. *23*, 1173–1180. https://doi.org/10.1016/j.cub.2013.05.015.

12. Lu, M., van Tartwijk, F.W., Lin, J.Q., Nijenhuis, W., Parutto, P., Fantham, M., Christensen, C.N., Avezov, E., Holt, C.E., Tunnacliffe, A., et al. (2020). The structure and global distribution of the endoplasmic reticulum network are actively regulated by lysosomes. Sci. Adv. *6*, eabc7209. https://doi.org/10.1126/sciadv.abc7209.

13. Kim, T.J., Joo, C., Seong, J., Vafabakhsh, R., Botvinick, E.L., Berns, M.W., Palmer, A.E., Wang, N., Ha, T., Jakobsson, E., et al. (2015). Distinct mechanisms regulating mechanical force-induced Ca^{2+} signals at the plasma membrane and the ER in human MSCs. eLife *4*, e04876. https://doi.org/10.7554/eLife.04876.

14. Haustrate, A., Prevarskaya, N., and Lehen'kyi, V. (2020). Role of the TRPV Channels in the Endoplasmic Reticulum Calcium Homeostasis. Cells *9*, 317. https://doi.org/10.3390/cells9020317.

15. Cai, Y., Maeda, Y., Cedzich, A., Torres, V.E., Wu, G., Hayashi, T., Mochizuki, T., Park, J.H., Witzgall, R., and Somlo, S. (1999). Identification and Characterization of Polycystin-2, the PKD2 Gene Product. J. Biol. Chem. *274*, 28557–28565. https://doi.org/10.1074/jbc.274.40.28557.

16. Lee, N.S., Yoon, C.W., Wang, Q., Moon, S., Koo, K.M., Jung, H., Chen, R., Jiang, L., Lu, G., Fernandez, A., et al. (2020). Focused Ultrasound Stimulates ER Localized Mechanosensitive PANNEXIN-1 to Mediate Intracellular Calcium Release in Invasive Cancer Cells. Front. Cell Dev. Biol. *8*, 504. https://doi.org/10.3389/fcell.2020.00504.

17. Haase, K., and Pelling, A.E. (2015). Investigating cell mechanics with atomic force microscopy. J. R. Soc. Interface *12*, 20140970. https://doi.org/10.1098/rsif.2014.0970.

18. Sergides, M., Perego, L., Galgani, T., Arbore, C., Pavone, F.S., and Capitanio, M. (2021). Probing mechanotransduction in living cells by optical tweezers and FRET-based molecular force microscopy. Eur. Phys. J. Plus *136*, 316. https://doi.org/10.1140/epjp/s13360-021-01273-7.

19. Deisseroth, K. (2011). Optogenetics. Nat. Methods *8*, 26–29. https://doi.org/10.1038/nmeth.f.324.

20. Duan, L., Che, D., Zhang, K., Ong, Q., Guo, S., and Cui, B. (2015). Optogenetic control of molecular motors and organelle distributions in cells. Chem. Biol. *22*, 671–682. https://doi.org/10.1016/j.chembiol.2015.04.014.

21. Huang, P., Liu, A., Song, Y., Hope, J.M., Cui, B., and Duan, L. (2020). Optical Activation of TrkB Signaling. J. Mol. Biol. *432*, 3761–3770. https://doi.org/10.1016/j.jmb.2020.05.002.

22. Zhao, E.M., Suek, N., Wilson, M.Z., Dine, E., Pannucci, N.L., Gitai, Z., Avalos, J.L., and Toettcher, J.E. (2019). Light-based control of metabolic flux through assembly of synthetic organelles. Nat. Chem. Biol. *15*, 589–597. https://doi.org/10.1038/s41589-019-0284-8.

23. Hannanta-Anan, P., and Chow, B.Y. (2018). Optogenetic Inhibition of $G\alpha_q$ Protein Signaling Reduces Calcium Oscillation Stochasticity. ACS Synth. Biol. *7*, 1488–1495. https://doi.org/10.1021/acssynbio.8b00065.

24. Dowbaj, A.M., Jenkins, R.P., Williamson, D., Heddleston, J.M., Ciccarelli, A., Fallesen, T., Hahn, K.M., O'Dea, R.D., King, J.R., Montagner, M., et al. (2021). An optogenetic method for interrogating YAP1 and TAZ nuclear-cytoplasmic shuttling. J. Cell Sci. *134*, jcs253484. https://doi.org/10.1242/jcs.253484.

25. Inglés-Prieto, Á., Reichhart, E., Muellner, M.K., Nowak, M., Nijman, S.M.B., Grusch, M., and Janovjak, H. (2015). Light-assisted small-molecule screening against protein kinases. Nat. Chem. Biol. *11*, 952–954. https://doi.org/10.1038/nchembio.1933.

26. Kim, N.Y., Lee, S., Yu, J., Kim, N., Won, S.S., Park, H., and Heo, W.D. (2020). Optogenetic control of mRNA localization and translation in live cells. Nat. Cell Biol. *22*, 341–352. https://doi.org/10.1038/s41556-020-0468-1.

27. Nguyen, N.T., Huang, K., Zeng, H., Jing, J., Wang, R., Fang, S., Chen, J., Liu, X., Huang, Z., You, M.J., et al. (2021). Nano-optogenetic engineering of CAR T cells for precision immunotherapy with enhanced safety. Nat. Nanotechnol. *16*, 1424–1434. https://doi.org/10.1038/s41565-021-00982-5.

28. Niopek, D., Wehler, P., Roensch, J., Eils, R., and Di Ventura, B. (2016). Optogenetic control of nuclear protein export. Nat. Commun. *7*, 10624. https://doi.org/10.1038/ncomms10624.

29. Wang, X., Chen, X., and Yang, Y. (2012). Spatiotemporal control of gene expression by a light-switchable transgene system. Nat. Methods *9*, 266–269. https://doi.org/10.1038/nmeth.1892.

30. Hörner, M., Jerez-Longres, C., Hudek, A., Hook, S., Yousefi, O.S., Schamel, W.W.A., Hörner, C., Zurbriggen, M.D., Ye, H., Wagner, H.J., et al. (2021). Spatiotemporally confined red light-controlled gene delivery at single-cell resolution using adeno-associated viral vectors. Sci. Adv. *7*, eabf0797. https://doi.org/10.1126/sciadv.abf0797.

31. Song, Y., Huang, P., Liu, X., Zhao, Z., Wang, Y., Cui, B., and Duan, L. (2022). Light-inducible deformation of mitochondria in live cells. Cell Chem. Biol. *29*, 109–119.e3. https://doi.org/10.1016/j.chembiol.2021.05.015.

32. van Bergeijk, P., Adrian, M., Hoogenraad, C.C., and Kapitein, L.C. (2015). Optogenetic control of organelle transport and positioning. Nature *518*, 111–114. https://doi.org/10.1038/nature14128.

33. Kennedy, M.J., Hughes, R.M., Peteya, L.A., Schwartz, J.W., Ehlers, M.D., and Tucker, C.L. (2010). Rapid blue-light-mediated induction of protein interactions in living cells. Nat. Methods *7*, 973–975. https://doi.org/10.1038/nmeth.1524.

34. Duan, L., Hope, J., Ong, Q., Lou, H.Y., Kim, N., McCarthy, C., Acero, V., Lin, M.Z., and Cui, B. (2017). Understanding CRY2 interactions for optical control of intracellular signaling. Nat. Commun. *8*, 547. https://doi.org/10.1038/s41467-017-00648-8.

35. Che, D.L., Duan, L., Zhang, K., and Cui, B. (2015). The Dual Characteristics of Light-Induced Cryptochrome 2, Homo-oligomerization and Heterodimerization, for Optogenetic Manipulation in Mammalian Cells. ACS Synth. Biol. *4*, 1124–1135. https://doi.org/10.1021/acssynbio.5b00048.

36. Liu, H., Yu, X., Li, K., Klejnot, J., Yang, H., Lisiero, D., and Lin, C. (2008). Photoexcited CRY2 interacts with CIB1 to regulate transcription and floral initiation in Arabidopsis. Science *322*, 1535–1539. https://doi.org/10.1126/science.1163927.

37. Mallik, R., and Gross, S.P. (2004). Molecular motors: strategies to get along. Curr. Biol. *14*, R971–R982. https://doi.org/10.1016/j.cub.2004.10.046.

38. Deguchi, T., Iwanski, M.K., Schentarra, E.M., Heidebrecht, C., Schmidt, L., Heck, J., Weihs, T., Schnorrenberg, S., Hoess, P., Liu, S., et al. (2023). Direct observation of motor protein stepping in living cells using MINFLUX. Science *379*, 1010–1015. https://doi.org/10.1126/science.ade2676.

39. Strickland, D., Lin, Y., Wagner, E., Hope, C.M., Zayner, J., Antoniou, C., Sosnick, T.R., Weiss, E.L., and Glotzer, M. (2012). TULIPs: tunable, light-controlled interacting protein tags for cell biology. Nat. Methods *9*, 379–384. https://doi.org/10.1038/nmeth.1904.

40. Carreras-Sureda, A., Pihán, P., and Hetz, C. (2018). Calcium signaling at the endoplasmic reticulum: fine-tuning stress responses. Cell Calcium *70*, 24–31. https://doi.org/10.1016/j.ceca.2017.08.004.

41. Mattson, M.P., LaFerla, F.M., Chan, S.L., Leissring, M.A., Shepel, P.N., and Geiger, J.D. (2000). Calcium signaling in the ER: its role in neuronal plasticity and neurodegenerative disorders. Trends Neurosci. *23*, 222–229. https://doi.org/10.1016/s0166-2236(00)01548-4.

42. Chen, T.W., Wardill, T.J., Sun, Y., Pulver, S.R., Renninger, S.L., Baohan, A., Schreiter, E.R., Kerr, R.A., Orger, M.B., Jayaraman, V., et al. (2013). Ultrasensitive fluorescent proteins for imaging neuronal activity. Nature *499*, 295–300. https://doi.org/10.1038/nature12354.

43. Thastrup, O., Cullen, P.J., Drøbak, B.K., Hanley, M.R., and Dawson, A.P. (1990). Thapsigargin, a tumor promoter, discharges intracellular Ca2+ stores by specific inhibition of the endoplasmic reticulum Ca2(+)-ATPase. Proc. Natl. Acad. Sci. USA *87*, 2466–2470. https://doi.org/10.1073/pnas.87.7.2466.

44. Suzuki, J., Kanemaru, K., Ishii, K., Ohkura, M., Okubo, Y., and Iino, M. (2014). Imaging intraorganellar Ca^{2+} at subcellular resolution using CEPIA. Nat. Commun. *5*, 4153. https://doi.org/10.1038/ncomms5153.

45. O'Neil, R.G., and Heller, S. (2005). The mechanosensitive nature of TRPV channels. Pflugers Arch. *451*, 193–203. https://doi.org/10.1007/s00424-005-1424-4.

46. AbouAlaiwi, W.A., Takahashi, M., Mell, B.R., Jones, T.J., Ratnam, S., Kolb, R.J., and Nauli, S.M. (2009). Ciliary polycystin-2 is a mechanosensitive calcium channel involved in nitric oxide signaling cascades. Circ. Res. *104*, 860–869. https://doi.org/10.1161/CIRCRESAHA.108.192765.

47. Gunthorpe, M.J., Rami, H.K., Jerman, J.C., Smart, D., Gill, C.H., Soffin, E.M., Luis Hannan, S., Lappin, S.C., Egerton, J., Smith, G.D., et al. (2004). Identification and characterisation of SB-366791, a potent and selective vanilloid receptor (VR1/TRPV1) antagonist. Neuropharmacology *46*, 133–149. https://doi.org/10.1016/s0028-3908(03)00305-8.

48. Li, Y., Wright, J.M., Qian, F., Germino, G.G., and Guggino, W.B. (2005). Polycystin 2 interacts with type I inositol 1,4,5-trisphosphate receptor to modulate intracellular Ca^{2+} signaling. J. Biol. Chem. *280*, 41298–41306. https://doi.org/10.1074/jbc.M510082200.

49. Sammels, E., Devogelaere, B., Mekahli, D., Bultynck, G., Missiaen, L., Parys, J.B., Cai, Y., Somlo, S., and De Smedt, H. (2010). Polycystin-2 activation by inositol 1,4,5-trisphosphate-induced Ca^{2+} release requires its direct association with the inositol 1,4,5-trisphosphate receptor in a signaling microdomain. J. Biol. Chem. *285*, 18794–18805. https://doi.org/10.1074/jbc.M109.090662.

50. Dana, H., Mohar, B., Sun, Y., Narayan, S., Gordus, A., Hasseman, J.P., Tsegaye, G., Holt, G.T., Hu, A., Walpita, D., et al. (2016). Sensitive red protein calcium indicators for imaging neural activity. eLife *5*, e12727. https://doi.org/10.7554/eLife.12727.

51. Watson, P., and Stephens, D.J. (2005). ER-to-Golgi transport: form and formation of vesicular and tubular carriers. Biochim. Biophys. Acta *1744*, 304–315. https://doi.org/10.1016/j.bbamcr.2005.03.003.

52. Niu, L., Ma, T., Yang, F., Yan, B., Tang, X., Yin, H., Wu, Q., Huang, Y., Yao, Z.P., Wang, J., et al. (2019). Atlastin-mediated membrane tethering is critical for cargo mobility and exit from the endoplasmic reticulum. Proc. Natl. Acad. Sci. USA *116*, 14029–14038. https://doi.org/10.1073/pnas.1908409116.

53. Boncompain, G., Divoux, S., Gareil, N., de Forges, H., Lescure, A., Latreche, L., Mercanti, V., Jollivet, F., Raposo, G., and Perez, F. (2012). Synchronization of secretory protein traffic in populations of cells. Nat. Methods *9*, 493–498. https://doi.org/10.1038/nmeth.1928.

54. Jiang, J., and Hui, C.C. (2008). Hedgehog Signaling in Development and Cancer. Dev. Cell *15*, 801–812. https://doi.org/10.1016/j.devcel.2008.11.010.

55. Tang, X., Chen, R., Mesias, V.S.D., Wang, T., Wang, Y., Poljak, K., Fan, X., Miao, H., Hu, J., Zhang, L., et al. (2022). A SURF4-to-proteoglycan relay mechanism that mediates the sorting and secretion of a tagged variant of sonic hedgehog. Proc. Natl. Acad. Sci. USA *119*, e2113991119. https://doi.org/10.1073/pnas.2113991119.

56. Walter, P., and Ron, D. (2011). The Unfolded Protein Response: From Stress Pathway to Homeostatic Regulation. Science *334*, 1081–1086. https://doi.org/10.1126/science.1209038.

57. Jia, L.X., Zhang, W.M., Zhang, H.J., Li, T.T., Wang, Y.L., Qin, Y.W., Gu, H., and Du, J. (2015). Mechanical stretch-induced endoplasmic reticulum stress, apoptosis and inflammation contribute to thoracic aortic aneurysm and dissection. J. Pathol. *236*, 373–383. https://doi.org/10.1002/path.4534.

58. Li, H., Zhang, X.Y., Wu, T.J., Cheng, W., Liu, X., Jiang, T.T., Wen, J., Li, J., Ma, Q.L., and Hua, Z.C. (2013). Endoplasmic reticulum stress regulates rat mandibular cartilage thinning under compressive mechanical stress. J. Biol. Chem. *288*, 18172–18183. https://doi.org/10.1074/jbc.M112.407296.

59. Groenendyk, J., Agellon, L.B., and Michalak, M. (2021). Calcium signaling and endoplasmic reticulum stress. Int. Rev. Cell Mol. Biol. *363*, 1–20. https://doi.org/10.1016/bs.ircmb.2021.03.003.

60. Luo, S., Baumeister, P., Yang, S., Abcouwer, S.F., and Lee, A.S. (2003). Induction of Grp78/BiP by translational block: activation of the Grp78 promoter by ATF4 through and upstream ATF/CRE site independent of the endoplasmic reticulum stress elements. J. Biol. Chem. *278*, 37375–37385. https://doi.org/10.1074/jbc.M303619200.

61. Pakos-Zebrucka, K., Koryga, I., Mnich, K., Ljujic, M., Samali, A., and Gorman, A.M. (2016). The integrated stress response. EMBO Rep. *17*, 1374–1395. https://doi.org/10.15252/embr.201642195.

62. Levskaya, A., Weiner, O.D., Lim, W.A., and Voigt, C.A. (2009). Spatiotemporal control of cell signalling using a light-switchable protein interaction. Nature *461*, 997–1001. https://doi.org/10.1038/nature08446.

63. Kaberniuk, A.A., Shemetov, A.A., and Verkhusha, V.V. (2016). A bacterial phytochrome-based optogenetic system controllable with near-infrared light. Nat. Methods *13*, 591–597. https://doi.org/10.1038/nmeth.3864.

64. Zhou, Y., Kong, D., Wang, X., Yu, G., Wu, X., Guan, N., Weber, W., and Ye, H. (2022). A small and highly sensitive red/far-red optogenetic switch for applications in mammals. Nat. Biotechnol. *40*, 262–272. https://doi.org/10.1038/s41587-021-01036-w.

65. Nijenhuis, W., van Grinsven, M.M.P., and Kapitein, L.C. (2020). An optimized toolbox for the optogenetic control of intracellular transport. J. Cell Biol. *219*, e201907149. https://doi.org/10.1083/jcb.201907149.

66. Arguin, G., Caron, A.Z., Elkoreh, G., Denault, J.B., and Guillemette, G. (2010). The transcription factors NFAT and CREB have different susceptibilities to the reduced Ca2+ responses caused by the knock down of inositol trisphosphate receptor in HEK 293A cells. Cell. Physiol. Biochem. *26*, 629–640. https://doi.org/10.1159/000322330.

67. Lu, J., Boheler, K.R., Jiang, L., Chan, C.W., Tse, W.W., Keung, W., Poon, E.N., Li, R.A., and Yao, X. (2018). Polycystin-2 Plays an Essential Role in Glucose Starvation-Induced Autophagy in Human Embryonic Stem Cell-Derived Cardiomyocytes. Stem Cells *36*, 501–513. https://doi.org/10.1002/stem.2764.

68. Grünweller, A., Wyszko, E., Bieber, B., Jahnel, R., Erdmann, V.A., and Kurreck, J. (2003). Comparison of different antisense strategies in mammalian cells using locked nucleic acids, 2′-O-methyl RNA, phosphorothioates and small interfering RNA. Nucleic Acids Res. *31*, 3185–3193. https://doi.org/10.1093/nar/gkg409.

69. Schneider, C.A., Rasband, W.S., and Eliceiri, K.W. (2012). NIH Image to ImageJ: 25 years of image analysis. Nat. Methods *9*, 671–675. https://doi.org/10.1038/nmeth.2089.

STAR★METHODS

KEY RESOURCES TABLE

REAGENT or RESOURCE	SOURCE	IDENTIFIER
Antibodies		
Rabbit anti-BiP	Proteintech	Cat#11587-1-AP; RRID: AB_2119855
Rabbit anti-XBP1s	Cell Signaling Technology	Cat#12782; RRID: AB_2687943
Rabbit anti-eIF2α	Abclonal	Cat#A0764; RRID: AB_2757387
Rabbit anti-peIF2α	Thermo Fisher Scientific	Cat#44-728G; RRID:AB_2533736
Rabbit anti-GAPDH	Cell Signaling Technology	Cat#5174; RRID: AB_10622025
Rabbit anti-Tubulin	Cell Signaling Technology	Cat#2128; RRID: AB_823664
Bacterial and virus strains		
XL10-Gold Competent Cells	Agilent	Cat#200315
Chemicals, peptides, and recombinant proteins		
DMEM	Thermo Fisher Scientific	Cat#21969035
Fetal bovine serum	Thermo Fisher Scientific	Cat#A5256701
Trypsin EDTA	Thermo Fisher Scientific	Cat#25300062
Penicillin-Streptomycin	Thermo Fisher Scientific	Cat#15140122
Poly-L-Lysine	Sigma Aldrich	CAS 25988-63-0
Thapsigargin	Sigma Aldrich	CAS 67526-95-8
SB-366791	Sigma Aldrich MedChemExpress	CAS 472981-92-3
Xestospongin C	Sigma Aldrich	CAS 88903-69-9
BAPTA-AM	Abcam	CAS 126150-97-8
EGTA-AM	MedChemExpress	CAS 99590-86-0
Capsaicin	Sigma Aldrich	CAS 404-86-4
Calcium-/Magnesium- Hanks' Balanced Salt Solution	Thermo Fisher Scientific	Cat#14175095
HEPES	Thermo Fisher Scientific	Cat#15630080
ATP disodium salt hydrate	Sigma Aldrich	CAS 34369-07-8
Biotin	Sigma Aldrich	CAS 58-85-5
Cycloheximide	Sigma Aldrich	CAS 66-81-9
Formaldehyde	Thermo Fisher Scientific	Cat#28908
RIPA buffer	Thermo Fisher Scientific	Cat#89900
PVDF membrane	Bio-Rad	Cat#1620174
Bovine Serum Albumin (BSA)	Bio-Rad	Cat#5000206
Western ECL Substrate	Bio-Rad	Cat#1705060
Critical commercial assays		
In-Fusion® HD Cloning Kit	Takara Bio	Cat#638920
CloneAmp™ HiFi PCR Premix	Takara Bio	Cat#639298
GeneArt™ Gibson Assembly HiFi Master Mix	Thermo Fisher Scientific	Cat#A46628
Lipofectamine™ 3000 Transfection Reagent	Thermo Fisher Scientific	Cat#3000015
LipofectamineTM RNAiMax Reagent	Thermo Fisher Scientific	Cat#13778030
BCA Protein Assay	Thermo Fisher Scientific	Cat#23225
Experimental models: Cell lines		
C. aethiops: COS-7 cells	ATCC	CVCL_0224
Human: HeLa cells	ATCC	CVCL_0030
Human: U2OS cells	ATCC	CVCL_0042
Human: PC3 cells	ATCC	CVCL_0035

(*Continued on next page*)

Continued

REAGENT or RESOURCE	SOURCE	IDENTIFIER
Oligonucleotides		
siRNA targeting sequence: IP3R (CCGAGAUGACAAGAAGAACAAGUUU)	Arguin et al.[66]	N/A
shRNA targeting sequence: PKD2 (CCAGGACUUGAGAGAUGAAAT)	Lu et al.[67]	N/A
shRNA targeting sequence: TRPV1 (GCGCAUCUUCUACUUCAACTT)	Grünweller et al.[68]	N/A
Recombinant DNA		
CRY2-tdTomato-Sec61β	This paper	N/A
KIF5A-GFP-CIBN	Duan et al.[20]	RRID: Addgene_102252
KIF5A-CIBN	Duan et al.[20]	RRID: Addgene_102251
Tau-GFP	This paper	N/A
KIF1A-GFP-CIBN	This paper	N/A
KIF5B-GFP-CIBN	This paper	N/A
KIF5C-GFP-CIBN	This paper	N/A
KIF1A-CIBN	This paper	N/A
KIF5B-CIBN	This paper	N/A
KIF5C-CIBN	This paper	N/A
mCh-Sec61β	This paper	N/A
ePDZ-tdTomato-Sec61β	This paper	N/A
KIF5A-GFP-LOVpep	This paper	N/A
KIF5A-LOVpep	This paper	N/A
CRY2-tdTomato-CB5	This paper	N/A
CRY2-Sec61β	This paper	N/A
CRY2(D387A)-tdTomato-Sec61β	This paper	N/A
CRY2(D387A)-GFP-Sec61β	This paper	N/A
Str-KDEL_SBP-GFP-ShhN	Tang et al.[55]	N/A
CIBN-GFP-ppKin14VIb	This paper	N/A
CIBN-ppKin14VIb	This paper	N/A
ER-GFP	This paper	N/A
mCh-Lamin	This paper	N/A
LAMP1-mCh	This paper	N/A
PEX-mCh	This paper	N/A
mCh-Miro1	This paper	N/A
Software and algorithms		
ImageJ	Schneider et al.[69]	https://imagej.nih.gov/ij/
GraphPad Prism	GraphPad software Inc	https://www.graphpad.com/scientific-software/prism/
THUNDER imaging system	Leica Microsystems	https://www.leica-microsystems.com/products/thunder-imaging-systems/

RESOURCE AVAILABILITY

Lead contact

Further information and requests for resources and reagents should be directed to the Lead Contact, Liting Duan (ltduan@cuhk.edu.hk)

Materials availability

Plasmid constructs for KIF5A-GFP-CIBN (Addgene#102252) and KIF5A-CIBN (Addgene#102251) used in this study are available on Addgene (http://www.addgene.org). The plasmid Str-KDEL_SBP-EGFP-ShhN was a gift from Professor Yusong Guo from the Hong

Kong University of Science and Technology. Cloning methods for other plasmid constructs based on the available plasmids are described in the method details section. All materials generated in this study are available from the lead contact with a completed Material Transfer Agreement.

Data and code availability

This study did not generate/analyze any standardized datatypes or computational datasets/code. Any additional information required to reanalyze the data reported in this paper is available from the lead contact upon request.

EXPERIMENTAL MODEL AND SUBJECT PARTICIPANT DETAILS

Cell lines

COS-7 (ATCC® CRL-1651™; RRID: CVCL_0224) cells, HeLa (ATCC® CCL-2™; RRID: CVCL_0030) cells, U2OS (ATCC® HTB-96™; RRID: CVCL_0042) cells, and PC3 (ATCC® CRL-1435™; RRID: CVCL_0035) cells were all cultured in DMEM medium (Thermo Fisher Scientific) supplemented with 10% FBS (fetal bovine serum, Thermo Fisher Scientific) and 1% P/S (Penicillin-Streptomycin, Thermo Fisher Scientific). All cultures were maintained at 37°C in a 5% CO_2 environment.

METHOD DETAILS

Plasmid Construction

All the plasmids used in this study were cloned in the mammalian expression vector pEGFPN1 or pmCherryC1 using In-fusion (Clontech) or ligation (Thermo Fisher Scientific) method. Arabidopsis thaliana cryptochrome 2 (CRY2, the photolyase homology region, a.a. 1-498) and its binding partner CIBN (N-terminus of Cryptochrome-Interacting Basic-helix-loop-helix 1, a.a. 1-170) were used. CRY2-tdTomato-Sec61β was made by fusing CRY2, tdTomato and Sec61β using In-Fusion. KIF5A-GFP-CIBN and KIF5A-CIBN were from the previous work.[20] Tau-GFP was constructed by replacing YFP in Tau-YFP with GFP using ligation. Motor domain of rat KIF1A and human KIF5B and human KIF5C were inserted into KIF5A-GFP-CIBN and replaced KIF5A to make KIF1A-GFP-CIBN, KIF5B-GFP-CIBN and KIF5C-GFP-CIBN respectively using In-Fusion. KIF1A-CIBN, KIF5B-CIBN and KIF5C-CIBN were made by replacing KIF5A in KIF5A-CIBN with KIF1A, KIF5B and KIF5C respectively using In-Fusion. mCh-Sec61β was constructed by removing CRY2 in CRY2-mCh-Sec61β using In-Fusion. ePDZ-tdTomato-Sec61β was made by replacing CRY2 in CRY2-tdTomato-Sec61β with ePDZ using Infusion. KIF5A-GFP-LOVpep and KIF5A-LOVpep were made by replacing CIBN in KIF5A-GFP-CIBN and KIF5A-CIBN with LOVpep respectively using Gibson Assembly (Thermo Fisher Scientific). CRY2-tdTomato-CB5 was made by inserting the transmembrane domain of CB5 into CRY2-tdTomato-Sec61β to replace Sec61β using In-Fusion. CRY2-GFP-Sec61β was constructed by replacing tdTomato in CRY2-tdTomato-Sec61β by ligation. CRY2-Sec61β was made by removing tdTomato in CRY2-tdTomato-Sec61β using In-Fusion. CRY2(D387A)-tdTomato-Sec61β and CRY2(D387A)-GFP-Sec61β was constructed by replacing CRY2 with its unfunctional mutant CRY2(D387A) in CRY2-tdTomato-Sec61β and CRY2-GFP-Sec61β respectively via In-Fusion. Truncated ppKin14VIb (a.a. 861-1321) were synthesized by GenScript Biotech Corporation. CIBN-ppKin14VIb and CIBN-GFP-ppKin14VIb were made by replacing GFP-Sec61β and Sec61β in CIBN-GFP-Sec61β[34] with ppKin14VIb respectively via In-Fusion. ER-GFP was made by fusing GFP and a KDEL ER retention sequence using In-Fusion. All vectors were linearized by restriction enzymes (Thermo Fisher). All inserted sequences were amplified by PCR using CloneAmp™ HiFi PCR Premix (Takara).

Cell culture and transfection

Cells were seeded on Poly-L-Lysine (Sigma Aldrich) coated 35 mm confocal dishes (SPL) 1-2 days before transfection. All cells were transfected with desired DNA plasmids using Lipofectamine 3000 Reagent Kit (Thermo Fisher Scientific). Transfected cells were allowed to recover and express the desired proteins overnight in a complete culture medium before imaging.

Fluorescence live cell imaging

The live imaging and simultaneous photostimulation of cells were performed on an epifluorescence microscope (Leica DMi8S, Thunder Imager, equipped with the Infinity Scanner) with an on-stage CO_2 incubator and a motorized stage. An adaptive focus control was used during the whole imaging process to keep the region of interest in focus. Imaging experiments were conducted one day after cell transfection. For blue-light stimulation, pulsed 470 nm blue light from LED light source (Lumencor, 100 to 200 ms pulse duration at 1 s or 2 s intervals at 48, 240, or 1200 mW/cm^2) was used for GFP imaging and to initiate optogenetic protein interactions. For tdTomato or mCherry imaging, pulsed 550 nm/575 nm green light from LED light source (200 ms pulse duration) was used. Laser scanning (Leica Infinity Scanner) was used for blue light illumination in target subcellular areas, where a 488 nm blue light laser was used to scan a selected area to induce optogenetic protein interactions. THUNDER (Leica), a computational clearing method, was used to process fluorescence images of the ER network to minimize background noise. For Figure S1D, the images were acquired by ZEISS Elyra 7 with Lattice SIM.[2]

Treatments with drugs or with Ca^{2+}-free medium

Thapsigargin (Sigma-Aldrich), SB-366791 (Sigma-Aldrich and MedChemExpress), Xestospongin C (Sigma-Aldrich), BAPTA-AM (Abcam), EGTA-AM (MedChemExpress) and Capsaicin (Sigma-Aldrich) were respectively dissolved in DMSO and diluted in the normal culture medium before being treated to cells. Cells were transfected with desired plasmids one day before drug treatment and

imaging. Cells were treated with 3 μM Thapsigargin for 30 min to block SERCA, or with 3 μM SB-366791 for 1 h to inhibit TRPV1 channels, or with 5 μM Xestospongin C for 1 h to inhibit IP3R channels, or with 50 μM BAPTA-AM or EGTA-AM for 30 min to chelate cytosolic Ca^{2+} in LIMER-induced Ca^{2+} release and ER-to-Golgi transport experiments. In ER stress experiments, cells were treated with 1 μM Thapsigargin or 50 μM BAPTA-AM for 10 h.

Ca^{2+}-free medium is composed of Calcium-/Magnesium- Hanks' Balanced Salt Solution (HBSS) complemented with 10 mM HEPES (Thermo Fisher Scientific). Pre-warmed Ca^{2+}-free medium replaces all normal culture medium before imaging.

Knockdown of PKD2, TRPV1, and IP3R3 in COS-7 cells

To knock down the expression of IP3R3, IP3R3 targeted small interfering RNAs (sense strand: 5′-CCGAGAUGACAAGAAGAACAA GUUU-3′)[66] labelled with Cyanine5 (Cy5) at the 5′-end of the sense siRNA strand were purchased from Sangon Biotech (Shanghai) Co., Ltd. Transfection of siRNA was performed using LipofectamineTM RNAiMax Reagent (Thermo Fisher Scientific) according to the manufacturers' protocol, and cells were analyzed 48h after siRNA transfection. To knock down the expression of PKD2 and TRPV1, shRNA cassettes were cloned downstream of the human polymerase III U6 promoter. Transfection was performed using Lipofectamine 3000 reagent and cells were analyzed 48h after shRNA transfection. The shRNA targeting sequences were as follows: PKD2 shRNA (5'-CCAGGACUUGAGAGAUGAAAU-3'),[67] TRPV1 shRNA (5'-GCGCAUCUUCUACUUCAACTT-3').[68] qPCR was used to confirm mRNA level after knockdown.

ATP-induced Ca^{2+} Release from ER

Cells were transfected with GCamP6 before imaging and treatment. ATP disodium salt hydrate (Sigma-Aldrich) was dissolved in milliQ water to make a 10 mM stock solution. The solution was further diluted to 20 μM in Ca^{2+}-free HBSS. Before ATP was given to the cells, the original culture medium was completely discarded and replaced by 200 μL of Ca^{2+}-free HBSS. For drug treatment groups, drugs of corresponding concentrations described in previous sections were added to the cell cultures. The cells were then placed under the microscope for fluorescence imaging. 10 to 20 s after the start of the imaging, 200 μL of 20 μM ATP solution was directly added into 200 μL medium to induce calcium release from ER to the cytosol. Changes in the fluorescence intensity of GCaMP6 were recorded.

Retention Using Selective Hook (RUSH) Transport Assay and quantification

COS-7 cells were seeded on 35 mm confocal dishes and transfected with RUSH and LIMER plasmids. 100 μg/mL cycloheximide (Sigma-Aldrich), the protein synthesis inhibitor, was added 2 h before biotin addition. Once 40 μM biotin (Sigma-Aldrich) was added, cells were illuminated with 1 mW/cm^2 intermittent blue light (1 s on/ 4 s off) for 15 min using a custom-built LED array inside a CO_2 incubator. Another set of transfected cells was kept in the dark as a control group. Cells were then fixed with 4% paraformaldehyde (Thermo Fisher Scientific Pierce™ 16% formaldehyde, methanol-free) prior to imaging. For quantification, we chose 4 fixed samples for each group from 4 independent experiments with both images acquired from tdTomato and GFP channels. Among all the co-transfected cells, we counted the ratios of cells with GFP signals accumulated at the Golgi area (represented by bright dots near the nucleus) 15 min after biotin addition in each experimental condition. The quantification was performed by individuals who were blind to all the experimental conditions.

Immunoblotting

COS-7 cells seeded in 6-well culture plates were transfected with desired DNA plasmids or treated with desired drugs and incubated for indicated durations. For short-term light illumination, cells were exposed to 1 mW/cm^2 intermittent blue light (1 s on/ 4 s off) for 5, 10, or 30 min using a custom-built LED array inside a CO_2 incubator, while another set of cells was incubated in dark as a control. For long-term light illumination, cells were exposed to 1 mW/cm^2 intermittent blue light at 4 s on/4 min off to decrease possible photo-toxicity for 1, 5, and 10 hours, while another set of cells was incubated in dark as a control. Total proteins were extracted by RIPA buffer (25 mM Tris HCl, 150 mM NaCl, 1% NP-40, 1% sodium deoxycholate, 0.1% SDS) containing protease and phosphatase inhibitor cocktails (Sigma) and quantified using the BCA Protein Assay (Thermo Fisher Scientific). Protein samples were separated by SDS-PAGE gels, transferred onto PVDF membranes (Bio-Rad), and blocked with 5% BSA in TBST buffer (Bio-Rad) at room temperature for 1h. Then PVDF membranes were incubated with anti-BiP (Proteintech 11587-1-AP), anti-XBP1s (CST 12782), anti-eIF2α (Abclonal A0764), anti-peIF2α (Thermo Fisher Scientific 44728), anti-GAPDH (CST 5174) and anti-tubulin (CST 2128) at 4°C overnight, washed in TBST buffer, and then incubated with HRP-conjugated secondary antibody (CST 7074) at room temperature for 1h. After washing three times in TBST, the protein bands were visualized by chemiluminescence (Western ECL Substrate, Bio-Rad) using a ChemiDoc imaging system.

QUANTIFICATION AND STATISTICAL ANALYSIS

Measurement of light-induced ER tubule elongation

Measurement of the maximal lengths and extending speeds of ER tubules was done on raw fluorescence images using ImageJ. All selected ER tubules could be individually identified and tracked throughout the time lapse of the measurement. The maximum length of the tubule was defined as the longest a tubule could reach before halting or retraction. Average speed of tubule elongation was calculated as the quotient of maximum length and time interval (in seconds). All data fitting and analysis was performed using Prism 7 (GraphPad).

Data Analysis for Ca^{2+} change

Alterations of cytosolic Ca^{2+} concentration were reported by relative changes in fluorescence intensity of calcium indicators, GCaMP6 or jRGECO1a or G-CEPIA1er. When measuring changes in Ca^{2+} level during light-induced mechanostimulation, cells with significant deformation after blue light stimulation were selected for analysis. When measuring changes in fluorescence signal in ATP treated groups, all the cells were selected for analysis. The average intensities of fluorescence signals of individual cells at each time point were measured by ImageJ. A region with no cell or other signal source was measured as the background fluorescence intensity for each selected image. Actual fluorescence intensity was defined as measured intensity deducted by background intensity. Then the intensity was normalized by the value from the same cell at the time point right before ATP treatment or blue light stimulation. Results were collectively analyzed to generate graphs of Ca^{2+} kinetics with each point showing mean ± SEM, and of maximum Ca^{2+} change with a bar showing general mean ± SEM

Statistical methods

Sample sizes were determined on the basis of previous experience in similar experiments. All statistics were performed using Prism 7 (GraphPad). First, datasets were tested for normal distribution using D'Agostino–Pearson normality test (significance value of 0.05). If a dataset failed this test, a non-parametric test was chosen to compare the significance of difference between groups (Mann–Whitney U test or Kruskal-Wallis test). For normally distributed datasets, a parametric test was chosen to compare two datasets (Student's t-test or one-way ANOVA). For each dataset, at least 2 independent sets of experiments were conducted. For a detailed description of statistical tests used and exact P values, please see Table S1.